# High-Throughput Estimation of Crop Traits

*A review of ground and aerial phenotyping platforms*

XIULIANG JIN, PABLO J. ZARCO-TEJADA, URS SCHMIDHALTER, MATTHEW P. REYNOLDS, MALCOLM J. HAWKESFORD, RAJEEV K. VARSHNEY, TAO YANG, CHENWEI NIE, ZHENHAI LI, BO MING, YONGGUI XIAO, YONGDUN XIE, AND SHAOKUN LI

xxxxx

Crop yields need to be improved in a sustainable manner to meet the expected worldwide increase in population over the coming decades as well as the effects of anticipated climate change. Recently, genomics-assisted breeding has become a popular approach to food security; in this regard, the crop breeding community must better link the relationships between the phenotype and the genotype. While high-throughput genotyping is feasible at a low cost, high-throughput crop phenotyping methods and data analytical capacities need to be improved.

High-throughput phenotyping offers a powerful way to assess particular phenotypes in large-scale experiments, using high-tech sensors, advanced robotics, and image-processing systems to monitor and quantify plants in breeding nurseries and field experiments at multiple scales. In addition, new bioinformatics platforms are able to embrace large-scale, multidimensional phenotypic datasets. Through the combined analysis of phenotyping and genotyping data, environmental responses and gene functions can now be dissected at unprecedented resolution. This will aid in finding solutions to currently limited and incremental improvements in crop yields.

*Digital Object Identifier 10.1109/MGRS.2020.2998816*
*Date of current version: 30 June 2020*

## BACKGROUND

Worldwide demand for food will increase through 2050 and beyond due to the increasing global human population. This represents a huge challenge to crop researchers and agricultural policymakers because current yield gain rates will not be sufficient for the demands of population growth, while climate change will make the difficulty even greater. Today's DNA sequencing, marker-assisted breeding, transgenic technology, genome-wide association study (GWAS) approaches, and quantitative trait loci (QTL) identification have been applied, to a limited extent, to improve crop yields [1]–[4].

While it is now relatively easy to select for monogenic traits, current genome sequence datasets have not been sufficiently mined for more genetically complex (multigenic) performance characteristics, at least in part because of the lack of crop phenotypic information collected from real-world field situations. Furthermore, traditional crop growth analysis often involves destructive sampling that is time-consuming and prone to measurement error. At present, the lack of traits amenable to high-throughput analysis restricts our ability to more thoroughly explore the quantitative genetic basis of complex characteristics correlated to crop's growth status, yield, and adaptation to environmental stress conditions. Thus, high-throughput phenotyping methods need to evolve to match the advances achieved in genotyping technologies.

The relatively recent availability of high-throughput crop phenotyping methods has influenced developments in crop selection and improvement [5], [6], and previous reviews have presented new opportunities for using ground and aerial phenotyping platforms that carry different sensors [7], [8]. Compared with other recent publications, this article comprehensively introduces recent applications of high-throughput ground and aerial phenotyping platforms for the measurement of crop phenotyping traits in the field. It demonstrates how high-throughput crop phenotyping can benefit breeders and agronomists and help narrow the genome–phenome gap. In particular, it discusses the disadvantages and advantages of different sensors and their applications and analyzes how to quickly and effectively estimate crop traits using ground and aerial phenotyping platforms.

## CROP PHENOTYPING

Phenotyping has been an important part of crop and elite-variety selection since humans found the best traits of plant species for domestication [9]. The term *phenotyping* does not have a completely clear-cut definition [10]. *Phenotyping* has been described as the use of protocols and methodologies to obtain a particular trait linked to plant functions and structures, with characteristics ranging from cells to whole plant levels [11]. An individual genotype represents all genetic characteristics, whereas a phenotype may include selected measured or all conceivable characteristics [12]. A complicated interaction between environmental conditions and genotypes leads to the phenotypic performance of crops [13]. One genotype can express various phenotypes due to plasticity in response to the environmental conditions in which plants grow. Thus, crop performance as an expression of genetic background requires an exploration of the relationship between phenotypes and genetics [14].

A common approach in crop breeding is to select the best genotype based on a phenotypic expression under various environmental conditions [15], [16]. Some traits (Table 1) considered in the field are green-area indexes (GAIs) [17]–[27], chlorophyll content [17], [18], [25], [27]–[33], nitrogen content [8], [17], [27], [29], [34]–[38], plant density at emergence [39]–[45], ear density [46]–[52], grain number and size [53]–[56], fraction of absorbed photosynthetically active radiation (FAPAR) [57]–[61], staygreen/senescence [62]–[66], crop dynamics monitoring [19], [67]–[73], phenology (e.g., at anthesis) [74]–[90], canopy coverage [62], [91]–[97], plant diseases and pests [8], [98]–[106], canopy height [107]–[112], canopy temperature [113]–[123], leaf rolling [124]–[126], leaf angle [112], [127]–[130], leaf wilting [131]–[133], lodging [134]–[145], chlorophyll fluorescence [6], [146]–[153], photosynthetic status [152], [154]–[160], biomass [23], [24], [107], [161]–[171], water content [114], [150], [172]–[179], grain quality [180]–[188], water use efficiency [168], [189]–[196], canopy structure [112], [197]–[204], weed infestation [41], [205]–[210], light use efficiency [211]–[218], nitrogen use efficiency [219]–[226], nitrogen nutrition index [227]–[233], and yield [170], [234]–[245].

Crop phenotyping aims to accurately and precisely obtain traits linked to crop growth status, yield, and resilience to environmental stress, at various scales ranging from cell to canopy [11]. To achieve this goal, scientists and engineers from crop breeding, electronic engineering, molecular biology, computer image processing, mathematics and statistics, and agronomy cooperate to develop high-throughput crop phenotyping platforms that are operational in the field. These crop phenotyping platforms use combinations of unmanned aerial vehicles (UAVs), robotics, remotely controlled systems, and image-processing and analysis technology to monitor crops' growth status and performance. Current field crop phenotyping platforms will continue to be developed for the simultaneous evaluation of multiple crop phenotyping traits for numerous plant species at various scales.

## SENSOR DEVELOPMENT FOR FIELD PHENOTYPING TRAITS

Enablers of the monitoring of crop phenotyping traits in the field include rapidly developing sensor technologies, including red–green–blue (RGB), multispectral, hyperspectral, and thermal cameras; photosynthesis and fluorescence sensors; stereo cameras; and lidar devices. These sensors are usually divided into leaf-level, near-canopy, and airborne sensors, based on their application scale for crop phenotyping traits. In general, RGB, multispectral, and hyperspectral technologies and thermal cameras are airborne sensors, while photosynthesis and fluorescence sensors are leaf-level instruments and stereo cameras and lidar are near-canopy devices.

### *LEAF-LEVEL SENSORS*

#### PHOTOSYNTHESIS SENSORS

Photosynthesis sensors are passive instruments used in the visible spectral region to measure the response of a crop photosynthesis status to different stress treatments [154]. This technology has been widely used in physiological and ecological studies [152], [159]. Photosynthesis sensors can be used to study the response of crop photosynthesis under different environmental conditions to better understand crop photosynthetic adaptation mechanisms [154]. As an example, the LI-COR 6400 is an open system, which means that transpiration and photosynthesis estimations are based on the differences in water ($H_2O$) and carbon dioxide ($CO_2$) in an air stream flowing through the leaf cuvette [155]. The net photosynthesis is computed using (1) [246]

**TABLE 1. SENSORS FOR ESTIMATING CROP PHENOTYPING TRAITS UNDER FIELD CONDITIONS, WITH THE LEVEL OF POTENTIAL APPLICATION.**

| | SENSOR | | | | | | | POTENTIAL APPLICATION LEVEL | | | | | | | | | | |
|---|---|---|---|---|---|---|---|---|---|---|---|---|---|---|---|---|---|---|
| PHENOTYPING TRAITS | RGB | MULTI/ HYPERSPECTRAL | THERMAL | PHOTOSYNTHESIS | FLUORESCENCE | STEREO | LIDAR | 1 | 2 | 3 | 4 | 5 | 6 | 7 | 8 | 9 | 10 | REFERENCE |
| GAI | ■ | ■ | ■ | | | | ■ | ■ | ■ | ■ | ■ | ■ | ■ | ■ | ■ | ■ | | [17]–[27] |
| Chlorophyll content | ■ | ■ | | | | | | ■ | ■ | ■ | ■ | ■ | ■ | | | | | [17], [18], [25], [27]–[33] |
| Nitrogen content | ■ | ■ | | | | | | ■ | ■ | ■ | ■ | ■ | ■ | | | | | [8], [17], [27], [29], [34]–[38] |
| Plant density at emergence | ■ | ■ | | | | | | ■ | ■ | ■ | ■ | ■ | ■ | ■ | ■ | | | [39]–[45] |
| Ear density | ■ | | | | | ■ | ■ | ■ | ■ | ■ | ■ | ■ | ■ | ■ | | | | [46]–[52] |
| Grain number and size | ■ | | | | | ■ | ■ | ■ | ■ | ■ | ■ | ■ | | | | | | [53]–[56] |
| FAPAR | ■ | ■ | | | | ■ | ■ | ■ | ■ | ■ | ■ | ■ | ■ | | | | | [57]–[61] |
| Staygreen/ senescence | ■ | ■ | | | | | | ■ | ■ | ■ | ■ | ■ | ■ | ■ | ■ | | | [62]–[66] |
| Crop dynamic monitoring | ■ | ■ | | | | ■ | ■ | ■ | ■ | ■ | ■ | ■ | ■ | | | | | [19], [67]–[73] |
| Phenology (e.g., anthe-sis) | ■ | ■ | | | | ■ | ■ | ■ | ■ | ■ | ■ | ■ | ■ | | | | | [74]–[90] |
| Canopy coverage | ■ | ■ | ■ | | | ■ | ■ | ■ | ■ | ■ | ■ | ■ | ■ | ■ | ■ | ■ | | [62], [91]–[97] |
| Plant diseases and pests | ■ | ■ | ■ | ■ | ■ | | | ■ | ■ | ■ | | | | | | | | [8], [98]–[106] |
| Canopy height | ■ | ■ | | | | ■ | ■ | ■ | ■ | ■ | ■ | ■ | ■ | ■ | ■ | | | [107]–[112] |
| Canopy temperature | | | ■ | | | | | ■ | ■ | ■ | ■ | ■ | ■ | | | | | [113]–[123] |
| Leaf rolling | ■ | ■ | ■ | | | ■ | ■ | ■ | ■ | ■ | ■ | ■ | | | | | | [124]–[126] |
| Leaf angle | ■ | | | | | ■ | ■ | ■ | ■ | ■ | ■ | ■ | ■ | | | | | [112], [127]–[130] |
| Leaf wilting | | ■ | ■ | | | | | ■ | ■ | ■ | ■ | ■ | | | | | | [131]–[133] |
| Lodging | ■ | ■ | ■ | ■ | ■ | ■ | ■ | ■ | ■ | ■ | ■ | ■ | ■ | ■ | ■ | | | [134]–[145] |
| Chlorophyll fluorescence | | ■ | | | ■ | | | ■ | ■ | ■ | ■ | ■ | | | | | | [6], [146]–[153] |
| Photosyn-thetic status | | | | ■ | ■ | | | ■ | ■ | ■ | ■ | ■ | | | | | | [152], [154]–[160] |
| Biomass | ■ | ■ | | ■ | ■ | ■ | ■ | ■ | ■ | ■ | ■ | ■ | ■ | ■ | ■ | | | [23], [24], [107], [161]–[171] |
| Water content | ■ | ■ | ■ | | | | | ■ | ■ | ■ | ■ | ■ | ■ | ■ | | | | [114], [150], [172]–[179] |
| Grain quality | | ■ | | | ■ | | | ■ | ■ | ■ | ■ | | | | | | | [180]–[188] |
| Water use efficiency | | ■ | ■ | ■ | | | | ■ | ■ | ■ | ■ | | | | | | | [168], [189]–[196] |
| Canopy structure | ■ | ■ | | | | ■ | ■ | ■ | ■ | ■ | ■ | ■ | | | | | | [112], [197]–[204] |
| Weed infestation | ■ | | | | | ■ | ■ | ■ | ■ | ■ | ■ | ■ | ■ | ■ | | | | [41], [205]–[210] |
| Light use efficiency | | | | ■ | ■ | | | ■ | ■ | ■ | ■ | | | | | | | [211]–[218] |
| Nitrogen use efficiency | ■ | ■ | | ■ | ■ | | | ■ | ■ | ■ | ■ | ■ | ■ | | | | | [219]–[226] |
| Nitrogen nutrition index | ■ | ■ | | | | | | ■ | ■ | ■ | ■ | ■ | ■ | | | | | [227]–[233] |
| Yield | ■ | ■ | ■ | ■ | ■ | ■ | ■ | ■ | ■ | ■ | ■ | ■ | ■ | ■ | ■ | | | [170], [234]–[245] |

$$sa = u_i c_i - u_o c_o, \quad (1)$$

where $s$ is the leaf area ($m^2$), $a$ is the assimilation rate ($mol\ CO_2\ m^{-2}\ s^{-1}$), $c_o$ and $c_i$ are the outgoing and incoming mole fractions of the $CO_2$ ($mol\ CO_2\ m^{-2}\ air^{-1}$), and $u_o$ and $u_i$ are the incoming and outgoing flow rates ($mol\ s^{-1}$). The transpiration is obtained using (2) [246]

$$sE = u_o w_o - u_i w_i sE = u, \quad (2)$$

where $E$ is the transpiration rate ($mol\ m^{-2}\ s^{-1}$) and $w_o$ and $w_i$ are the outgoing and incoming water mole fractions ($mol\ H_2O\ mol\ air^{-1}$).

The LI-COR 6400 contains a computing and storage section; an infrared $CO_2$ analyzer; and temperature, humidity, and light sensors. The moisture and $CO_2$ of the LI-COR 6400 instrument should be cleared and checked to obtain a value equal to zero to calibrate the sensor before measuring crop leaves [157]. Figure 1(e) shows an example of cotton measured from an LI-COR 6400 instrument. The exported calculated parameters include the photosynthetic rate, conductance to $H_2O$, intercellular $CO_2$ concentration, transpiration rate, and so forth [158]. These parameters can be used to carry out studies of crop growth analyses, gas exchanges, and stable isotope examinations [159]. At present, photosynthesis sensors do not provide any images and cannot be combined with ground and aerial imaging platforms [156]. The specific model, sensor parameters, details, estimated phenotyping traits, imaging environment, and limitations of the photosynthesis sensor are summarized in Table 2. New technologies will be required for rapid, image-based photosynthesis sensors to better explore the response of crop photosynthesis to environmental changes in the future.

## FLUORESCENCE SENSORS

Fluorescence sensors are passive or active in the ultraviolet, visible, and near-infrared spectral regions, which are sensitive to fluorescence signals [153]. They are commonly used to detect the resilience of the crop metabolic status in stressed environments [147]. The fluorescence sensor provides an image for exploring the spatial patterns of the leaf photosynthetic status [151] and for the early detection of crop stress symptoms, as influenced by diseases and pests [98]. Fluorescence is light that is emitted in the ultraviolet, visible, and near-infrared spectral wavelengths

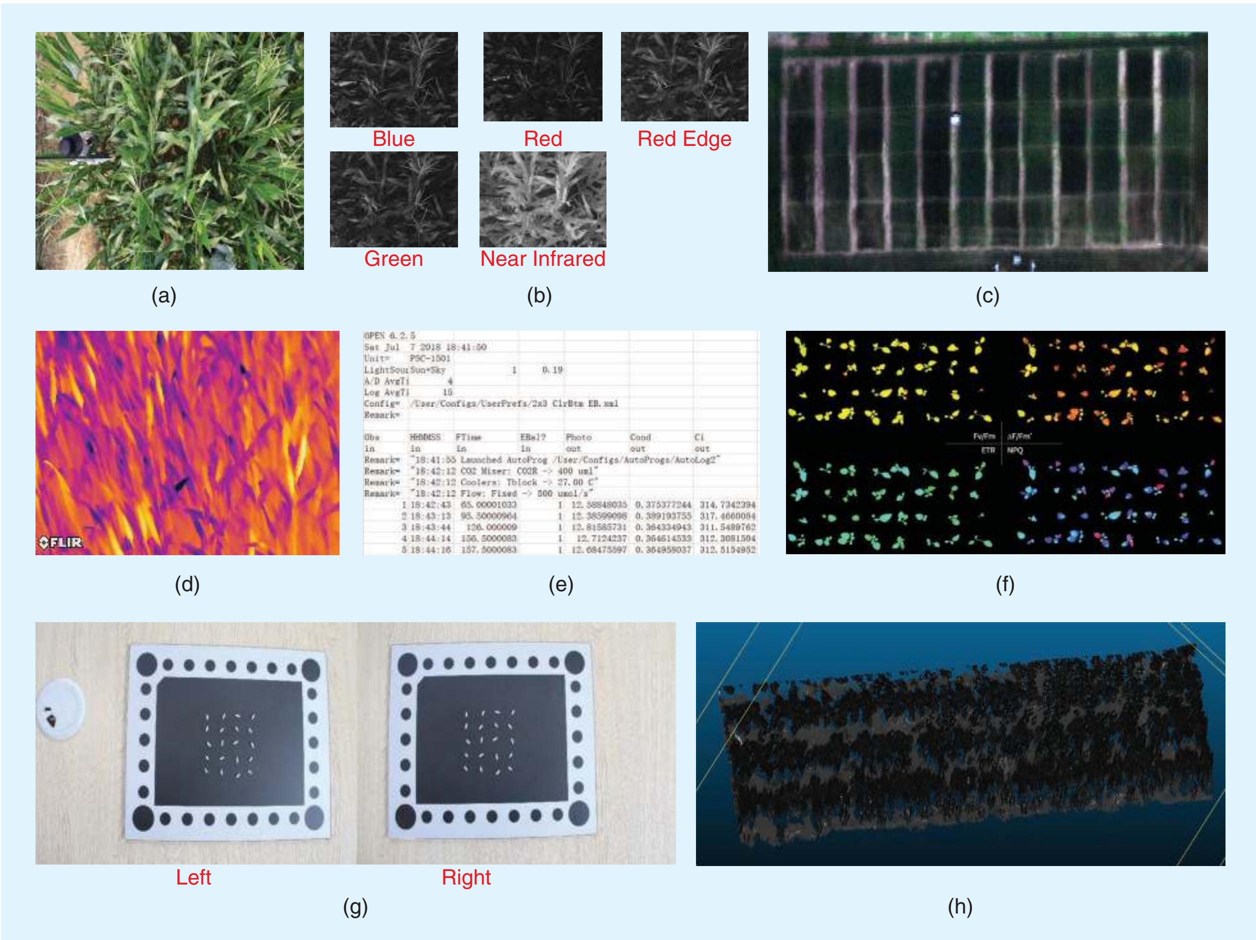


**FIGURE 1.** Example images from different sensors, including (a) an RGB camera, (b) a multispectral camera, (c) a hyperspectral camera, (d) a thermal camera, (e) a photosynthesis sensor, (f) a fluorescence sensor, (g) a stereo camera [254], and (h) lidar.

**TABLE 2. COMPARISON AND LIMITATIONS OF DIFFERENT SENSORS FOR FIELD CROP PHENOTYPING TRAITS.**

| SENSOR TYPE | MODEL | SENSOR PARAMETERS | DETAILS | PHENOTYPING TRAITS | IMAGING ENVIRONMENT | IMAGING TECHNIQUES | LIMITATIONS |
|---|---|---|---|---|---|---|---|
| Photosynthesis sensor | LI-COR 6400 | ✓ Sensor type: absolute, open-path, nondispersive infrared gas analyzer<br>✓ Bandwidth: 10 Hz<br>✓ Range: 0–3,100 $\mu$mol mol$^{-1}$ | Passive sensor at the visible spectral region | Plant diseases and pests, lodging, chlorophyll fluorescence, photosynthetic status, biomass, water use efficiency, light use efficiency, nitrogen use efficiency, nitrogen nutrition index, yield | Controlled environment; field | No | ✓ Sensors are costly.<br>✓ Measurements are time consuming.<br>✓ Only measured point data are obtained.<br>✓ It is not easy to measure at the canopy scale.<br>✓ No image.<br>✓ It is not possible to mount on field crop phenotyping platforms. |
| Fluorescence sensor | PlantExplorer | ✓ Sensor type: charge-coupled device<br>✓ Image resolution: 1.3 megapixels<br>✓ Spectral range: 350–1,000 nm<br>✓ Frame rate: 20 images per second | Passive or active sensor at the ultraviolet, visible, and near-infrared spectral regions | Plant diseases and pests, lodging, chlorophyll fluorescence, photosynthetic status, biomass, grain quality, light use efficiency, nitrogen use efficiency, nitrogen nutrition index, yield | Controlled environment; field | Fluorescence imaging | ✓ Difficult to measure at the canopy scale due to low signal-to-noise ratio.<br>✓ Difficult to implement on field crop phenotyping platforms.<br>✓ It will be strongly influenced by background noise. |
| Stereo camera | Stereolabs ZED | ✓ Sensor resolution: dual 4-megapixel sensors with 2-$\mu$m pixels<br>✓ Sensor format: native 16:9 format for a greater horizontal field of view<br>✓ Sensor size: 1/3-in backside illumination sensors with high low-light sensitivity | Camera with two or more lenses, with a separate image sensor for each lens | Ear density, grain number and size, FAPAR, crop dynamic monitoring, phenology, canopy coverage, canopy height, leaf rolling, leaf angle, lodging, biomass, canopy structure, weed infestation, yield | Controlled environment; field | 3D imaging | ✓ Experimental conditions influence its performance.<br>✓ Resolution of images is lower.<br>✓ Field application is limited.<br>✓ Sensor needs calibration before use. |
| Lidar | Sick LMS400-2000 | ✓ Light source: visible red light (650 nm)<br>✓ Laser class: 2<br>✓ Aperture angle: horizontal 70°<br>✓ Scanning frequency: 230–500 Hz<br>✓ Angular resolution: 0.1–1<br>✓ Working range: 0.7–3 m | Active sensor that detects the distance to a target from pulses of laser light | GAI, ear density, grain number and size, FAPAR, crop dynamic monitoring, phenology, canopy coverage, canopy height, leaf rolling, leaf angle, lodging, biomass, canopy structure, weed infestation, yield | Controlled environment; field | Laser imaging | ✓ Sensitive to small differences in path length.<br>✓ High cost of the sensor.<br>✓ Sensor should be integrated with GPS for georeferencing information.<br>✓ Data processing is time consuming. |

*Continued*

**TABLE 2. COMPARISON AND LIMITATIONS OF DIFFERENT SENSORS FOR FIELD CROP PHENOTYPING TRAITS.**

| SENSOR TYPE | MODEL | SENSOR PARAMETERS | DETAILS | PHENOTYPING TRAITS | IMAGING ENVIRONMENT | IMAGING TECHNIQUES | LIMITATIONS |
|---|---|---|---|---|---|---|---|
| Digital camera (RGB) | Sony Alpha 6000 | ✓ Sensor: Advanced Photo System Type C (23.5 × 15.6 mm)<br>✓ Aspect ratio: 3:2<br>✓ Image processing: Boinz X<br>✓ Image resolution: 6,000 × 4,000<br>✓ Focal length lens: 60 mm | ✓ Gray value [digital number (DN)]<br>✓ Color image<br>✓ Texture information | GAI, chlorophyll content, nitrogen content, plant density, ear density, grain number and size, FAPAR, staygreen/senescence, crop dynamic monitoring, phenology, canopy coverage, plant diseases and pests, canopy height, leaf rolling, leaf angle, leaf wilting, lodging, biomass, canopy structure, weed infestation, nitrogen use efficiency, nitrogen nutrition index, yield | Controlled environment; field | Visible light imaging | ✓ Limited to visual three spectral bands.<br>✓ Only relative value is obtained.<br>✓ Images do not carry out calibration.<br>✓ Effect of illumination condition on image acquisition quality limits image processing. |
| Multispectral camera | MicaSense RedEdge-M | ✓ Bands: blue (475 ± 20 nm), green (560 ± 20 nm), red (668 ± 10 nm), near infrared (840 ± 40 nm), red edge (717 ± 10 nm)<br>✓ Aspect ratio: 4:3<br>✓ Image resolution: 1,280 × 960<br>✓ Focal length lens: 5.4 mm | Several spectral bands of each pixel at the visible and infrared spectral regions | GAI, chlorophyll content, nitrogen content, plant density, FAPAR, staygreen/senescence, crop dynamic monitoring, phenology, canopy coverage, plant diseases and pests, canopy height, leaf rolling, leaf wilting, lodging, biomass, water content, grain quality, water use efficiency, canopy structure, nitrogen use efficiency, nitrogen nutrition index, yield | Controlled environment; field | Visible and near-infrared imaging | ✓ Limited to several spectral bands.<br>✓ Spectral data should be frequently calibrated using referenced objects.<br>✓ Effects of camera geometrics, illumination condition, and sun angle on the data signal. |
| Hyperspectral camera | Specim FX10 | ✓ Spectral range: 400–1,000 nm<br>✓ Spectral bands: 224<br>✓ Spectral full width at half maximum: 5.5 nm<br>✓ Spatial sampling: 1,024 pixels<br>✓ Frame rate: 330 frames per second, full frame<br>✓ Aperture: F/1.7<br>✓ Camera signal-to-noise ratio: 600:1 | Discrete or continuous spectral bands of each pixel at the visible and infrared spectral regions | GAI, chlorophyll content, nitrogen content, FAPAR, staygreen/senescence, crop dynamic monitoring, phenology, canopy coverage, plant diseases and pests, leaf rolling, leaf wilting, lodging, biomass, water content, grain quality, water use efficiency, canopy structure, nitrogen use efficiency, nitrogen nutrition index, yield | Controlled environment; field | Hyperspectral imaging | ✓ Image dataset processing is challenging.<br>✓ Price of the sensor is expensive.<br>✓ Spectral data should be frequently calibrated using referenced objects.<br>✓ Effects of camera geometrics, illumination condition, and sun angle on the data signal. |
| Thermal camera | Flir Vue Pro 336 | ✓ Spectral range: 7.5–13.5 $\mu$m<br>✓ Focal length lens: 6.8 mm<br>✓ Image resolution: 336 × 256<br>✓ Thermal imager: uncooled vanadium oxide microbolometer | Temperature of each pixel at the thermal spectral infrared regions | GAI, canopy coverage, plant diseases and pests, canopy temperature, leaf rolling, leaf wilting, lodging, water content, water use efficiency, yield | Controlled environment; field | Thermal imaging | ✓ Experimental conditions influence performance.<br>✓ Difficult to detect very small temperature differences.<br>✓ Price of the high-resolution sensors is expensive.<br>✓ Small-volume and low-weight sensors suffer during temperature shifts.<br>✓ Sensor needs to timely calibrated. |

during radiation absorption [148]. Irradiating chloroplasts with actinic or blue light will produce some reemission of absorbed light by chlorophyll [149]. Compared with incident radiation, the fraction of reemission light is variable and relies on the crop's ability to convert harvested light to metabolic activity [247]. The reemitted light is termed *fluorescence*, and it is a good indicator of a crop's capacity to assimilate actinic light [247].

Furthermore, the combination of actinic light and brief, saturating blue pulses can be used to measure the efficiency of photoassimilation, nonphotochemical quenching, and other physiological crop parameters [247]. Fluorescence sensors use a charge-coupled-device camera that is very sensitive to fluorescence signals, where fluorescence signals occur by illuminating crops with ultraviolet or visible light using pulsed lasers, pulsed flashlight lamps, or light-emitting diodes [150]. The image pixel value of the fluorescence indicators is presented by a false color code ranging from zero to one [248]. Ultraviolet illumination produces two kinds of fluorescence, that is, blue-to-green and red-to-far-red regions, which is the principle of multicolor fluorescence images [248]. This method can capture the simultaneous fluorescence emission from four spectral bands [blue (440 nm, F440), green (520 nm, F520), red (690 nm, F690), and far-red (740 nm, F740)] by excitation with a single wavelength [249]. The fluorescence sensor does not need to be calibrated before measuring crops, but it is better used under uniform illumination conditions to reduce the effect of the light source on the measurement results [250].

Figure 1(f) presents an example of soybeans provided through PlantExplorer, and the corresponding exporting fluorescence parameters include the initial fluorescence ($F_o$), maximum fluorescence ($F_m$), photosynthetic system 2 original light-energy conversion efficiency ($F_v/F_m$), photosynthetic quantum yield, photochemical-quenching coefficient, nonphotochemical-quenching coefficient, apparent electron transfer rate, and so forth [251]. These parameters can be used to carry out studies of crop stress analyses, photosynthetic functions, and chloroplast content estimations [250].

Current fluorescence sensors are focused mainly at the leaf scale. Chlorophyll fluorescence at the canopy scale is restricted by sensor and background noise, decreasing the signal-to-noise ratio [150]. Table 2 contains more information about photosynthesis sensor models, parameters, phenotype estimation traits, imaging environments, imaging techniques, and limitations. Therefore, fluorescence sensors are generally not available for integration with ground and aerial phenotyping platforms. However, chlorophyll fluorescence sensing on ground phenotyping platforms was used to assess the nitrogen status and biomass of wheat, barley, and colza [146], [147], [252]. There is a need for further development of fluorescence sensors and protocols for fluorescence image-based, high-throughput crop phenotyping to enhance field applications in the future.

## NEAR-CANOPY SENSORS

### STEREO CAMERAS

A stereo camera has two or more lenses, with separate imaging sensors for each [167]. Structures are observed in 3D because of the parallax effect of human eyes [253]. Due to the distance between a person's eyes, the two images formed at the fundi are basically similar but slightly different, and there is a certain disparity [130]. The brain then computes a 3D image. Stereo cameras with charge-coupled device chips take advantage of the parallax characteristics of both eyes [46]. In general, the stereo camera is very similar to the traditional digital camera but with two or more lenses. Some scientists use two identical, unmodified cameras to obtain 3D images [130], [254].

To maintain the accuracy and stability of a stereo camera, the device should be calibrated during experiments [254]. The calibration of a stereo camera is performed as follows:

1) The instrument needs to be tuned to obtain internal and external parameters and the homographic matrix.
2) The calibration results are used to correct the original image so that the two adjusted pictures are located on the same plane and parallel to each other.
3) The two corrected images must be matched according to the same pixel.

Figure 1(g) provides example rice seed images from a pair of cameras (Canon EOS 7D) [254]. The exported data of a stereo camera contain RGB images and a 3D structure [130], [254] that can be used to obtain crop growth and development information [130].

The model, parameters, estimated phenotypic traits, imaging environments, imaging techniques, and limitations of the stereo camera are presented in Table 2. The advantage of the stereo camera is that it provides 3D structures at a relatively low cost, but the spatial resolution is limited and sensitive to variable outdoor illumination conditions [247]. These restrictions have become major challenges for the stereo camera's application to crop phenotyping in the field. Currently, the stereo camera is used mostly to obtain the 3D structure of single plants; with it, estimating canopy-level traits in the field remains difficult [130]. Improvements in the stereo camera's resolution and sensitivity to illumination will be needed in the future.

### LIDAR

Lidar has an active sensor that determines the distance to an object using pulses of laser light in the 600–1,000-nm region [129]. Lidar is an Earth-observation technology that can directly obtain the 3D coordinates of object surface points through data such as positions, distances, and angles, and it realizes the extraction of the surface information and the reconstruction of the 3D scene [112]. Lidar includes a single-beam narrowband laser and a receiving system. The laser generates and emits a light pulse, which hits the target object and reflects back to a receiver [199].

The receiver accurately measures the propagation time of the light pulse from emission to reflection [112]. Because the pulse travels at the speed of light, the receiver always obtains a reflected pulse before the next one is sent. Given that the speed of light is known, the time of flight can be converted into a measurement of distance [200].

The laser itself has a very accurate ranging ability, and its ranging accuracy can reach the millimeter level. In general, an airborne lidar system integrates three technologies: laser scanning, GPS/differential GPS, and an inertial navigation system. This combination can locate with high accuracy a laser beam spot hitting an object [255]. The principle of measuring the ground from a flying carrier concerns the "two-way" time measurement method [200]. That is to say, we need to record only the time between a laser signal's emission and its return. Combined with other data, we can accurately calculate the *x*-, *y*-, and *z*-coordinates of the ground spot. Lidar does not need to be calibrated, but known referenced objects are necessary to accurately obtain crop structure information.

Figure 1(h) shows an example image of sunflowers that was acquired with a Sick LMS400. Lidar can provide a 3D point cloud to describe the crop canopy structure [129]. The point cloud can be used to monitor dynamic crop changes during the growing season [197], [200]. Table 2 describes a typical lidar model and its parameters, phenotype estimating traits, imaging environment, imaging techniques, and limitations. Compared with other sensors, lidar is less influenced by environmental conditions, and it has a relatively high estimation accuracy for several crop phenotyping traits because it is an active sensor [198]. However, the price of lidar is generally higher than that of passive sensors. Lidar is sensitive to small differences in the path length, although the data processing is more complex (Table 2). Lidar has been integrated with ground and aerial phenotyping platforms to estimate crop phenotyping traits [112], [197], [200], [220], [255]. However, in the future, the density of the achievable 3D point cloud needs to be increased to better describe 3D crop structures.

## *AIRBORNE SENSORS*

### RGB CAMERAS

RGB cameras record red, green, and blue spectral bands in the visible spectral regions [39]. An RGB camera produces digital images and can mimic human visible perception to obtain information for estimating crop phenotyping traits in plant breeding [74]. The most common implementation of RGB cameras is based on silicon sensors with charged-coupled devices or CMOS arrays that are very sensitive to visible bands of light and show images in 2D; this is the simplest imaging technique for crop phenotyping traits [247]. RGB camera images are typically shown in spatial matrices of intensity values (from zero to 255) corresponding to photon fluxes in blue, green, and red spectral bands of the visible region [46]. To obtain better high-quality RGB images, a color calibration plate is commonly used to adjust images using algorithms to reduce the effect of different illumination conditions on the photo quality [256], [257].

Figure 1(a) gives an example image of maize taken with a Sony Alpha 7 camera. The RGB camera can export images that include gray value, color, and texture information [39]. The applications of RGB cameras for crop phenotyping traits are shown in Tables 1 and 2, including GAI, plant density, ear density, FAPAR, canopy coverage, canopy height, leaf rolling, leaf angle, lodging, and so on, during the whole crop growing season. In addition, a typical camera model and its parameters, phenotype estimating traits, imaging environment, imaging techniques, and limitations are presented in Table 2. RGB cameras have been widely applied to evaluate crop phenotyping traits in the field to provide measurements at an affordable price [46], [47], [162], [164], [258].

Compared with other sensors, the advantage of the RGB camera relates to its affordable price and high-spatial-resolution imagery [237]. However, it remains a huge challenge to get good image segmentation results when adjacent plant leaves overlap [39]. In addition, the gray values and color information are limited to three visual spectral bands. New technologies are required to solve these shortcomings and improve the application of the RGB camera for crop phenotyping trait estimation [7]. Currently, a modified RGB camera [the so-called color–infrared (CIR) camera] with near-infrared, red, and green bands may be applied to obtain spectral vegetation images when it is radiometrically calibrated [259], [260]. The pseudonormalized-difference vegetation index (pseudo-NDVI) from a CIR camera has been applied for crop phenotyping [7], [258], [261], [262]. CIR cameras can be used to obtain high-spatial-resolution imagery with a limited number of wide spectral bands at a relatively low cost. However, CIR cameras may be unstable, and they have a limited application, as they are not designed for precise radiometric measurements [263].

### MULTISPECTRAL AND HYPERSPECTRAL CAMERAS

Multispectral and hyperspectral cameras depend on the interaction between solar radiation and crops [71]. The reflectance of single leaves or canopies is low in the visible spectral ranges (400–700 nm) because solar radiation is absorbed by leaf pigments (such as chlorophyll), with a peak of reflectance in the green spectral region of roughly 550 nm [45]. The reflectance (so-called red-edge region) is sharply increased with the transition from the visible to near-infrared spectral region [32]. A large fraction of the incident solar radiation is reflected by leaves because of scattering within the leaf structure and mesophyll in the near infrared (700–1,200 nm) region [24]. Furthermore, near-infrared radiation is transmitted from the upper to the lower leaves of the canopy, which can reflect solar radiation back to the upper section of the leaf cover [168]. Therefore, the leaf thickness and growth status as well as the canopy architecture primarily influence the reflectance pattern in this spectral region [27]. The reflectance is gradually decreased with increasing wavelengths of up to 2,500 nm because the absorption of solar radiation is increased by the water in crop leaves [59].

Multispectral cameras commonly include several spectral bands in the visible and infrared spectral regions [34]. Spectral bands are generally sensitive to leaf pigments and the leaf and canopy structure [45], [67]. Compared with their multispectral counterparts, hyperspectral cameras have a higher spectral resolution, with continuous or discrete spectral bands in the visible and infrared spectral regions [17], [264]. Hyperspectral bands are more sensitive to small changes in leaf pigments, such as carotenoids, chlorophyll a and b, and xanthophylls as well as leaf and canopy structures [265]. Multispectral or hyperspectral bands are used to obtain VIs through band calculations. More advanced methods based on radiative transfer model inversion techniques can also be employed [266].

To reduce the effects of illumination conditions on multispectral and hyperspectral cameras, radiometric image calibration should be carried out at each band [266]. First, several calibration targets ($1 \times 1$ m) that have different reflectance values are placed in the UAV flight area. Second, the digital number (DN) of each target is collected from UAV multispectral and hyperspectral images, and the corresponding actual reflectance of each target is also measured using, for example, an ASD spectroradiometer [166]. Third, the regression relationship between the reflectance and the DN value is established at each band image through empirical linear or nonlinear methods, and the DN value in the images is converted to the normalized reflectance using established regression relationship equations [71].

Figure 1(b) and (c) gives examples of maize and wheat images acquired with MicaSense RedEdge-M and Cubert UHD185 cameras, respectively. Multispectral and hyperspectral cameras can export images that include DN values and texture, reflectance, and color information [45]. Crop phenotyping trait estimations from multispectral and hyperspectral cameras are presented in Tables 1 and 2, including GAI, plant density, ear density, FAPAR, canopy coverage, staygreen/senescence, crop dynamics monitoring, phenology, plant diseases and pests, and so forth, across the whole crop growing season. The models, parameters, phenotype estimating traits, imaging environments, imaging techniques, and limitations of multispectral and hyperspectral cameras are detailed in Table 2.

The advantage of multispectral and hyperspectral cameras is that they have spectral information (except texture and color information) that could be better used to estimate crop phenotyping traits through fusion algorithms (this is an image process of integrating related information from two or more images into a single image and could be applied to acquire more useful information from the input images) [59], [115]. The application of multispectral and hyperspectral cameras in the field of crop phenotyping traits has attracted the attention of breeding programs [22], [103], [104], [267]. The main limitations concern the very large volume of data associated with spectral imagery and the generally more complex operation of hyperspectral cameras compared to multispectral and RGB cameras. These shortcomings impede their application and adaptation [36], [266].

In summary, multispectral cameras are mainly used for VI-based traits, due to the limited number of available bands, while hyperspectral cameras enable the calculation of more advanced crop phenotyping traits, such as photosynthetic status and fluorescence [265], [266]. With the rapid development of multispectral, hyperspectral, and computer image-processing technologies, cheaper multispectral and hyperspectral cameras will be developed and combined with high-performance graphics and computer-clustering technologies.

## THERMAL CAMERAS

Thermal cameras are used to measure infrared radiation in the thermal spectral infrared regions as a water stress indicator [115]. Thermal cameras operate in the spectral range from 3 to 14 $\mu$m, and their most-used spectral wavelengths are 3–5 $\mu$m and 7–14 $\mu$m, respectively [71], [266], [268]. The infrared radiation atmospheric transmission is very close to its maximum value in these two spectral ranges [121]. The thermal sensitivity of the spectral range from 3 to 5 $\mu$m is associated with higher energy levels than the spectral range from 7 to 14 $\mu$m, but using wavelengths of 7–14 $\mu$m has advantages for certain applications [269]. The wavelength ranges between 8 and 14 $\mu$m can reduce errors from the atmospheric absorption of infrared radiation for objects through longer atmospheric paths [269].

Thermal cameras should be calibrated to maintain the measurement accuracy and stability of their images. First, a thermal camera is preheated for roughly 20 min in the field before a UAV flight to reduce the temperature drift, and the automated nonuniformity correction is enabled during the data measurement [270]. Second, according to a thermal camera's preheating guidelines, one JPEG image of a blackbody radiometric background scene is taken, which is immediately obtained from one 14-b TIFF-format image of the same scene [235]. Third, the blackbody radiometric JPEG is loaded into FLIR Tools software, which provides options for imaging target-related parameters and environmental conditions, to execute a radiometric conversion [271]. At the same time, the air humidity and temperature are added from a weather station, along with the target distance (flight height) and object emissivity to obtain temperature values that are output in a text file [272]. The bias between the blackbody and the image temperature is determined. Finally, each pixel's radiometric value in the 14-b TIFF image is correlated to the corresponding value in the text file, with a linear model being used as a radiometric conversion regression equation, and the radiometric value in the images is transformed into the temperature using the established regression relationship equation [235].

Figure 1(d) provides an example image of wheat obtained using a FLIR SC620 camera. Thermal cameras export images that include the temperature, radiometric values, and texture information [271]. The application of a thermal camera to crop phenotyping trait estimation is illustrated in Tables 1 and 2. Thermal camera models, parameters, phenotype estimating traits, imaging environments, imaging techniques, and limitations are shown in Table 2. In recent years, thermal cameras with a high thermal sensitivity have been widely applied to estimate crop growth statuses under water stress conditions [116], [120], [266], [273]. Spatial patterns obtained from thermal images may be used to carry out image segmentation to differentiate stressed and unstressed vegetation by using image-processing algorithms [273]. The cost of thermal cameras is generally higher than for multispectral cameras, and lightweight models are typically thermally unstable due to changing ambient conditions [268]. Thermal cameras can be utilized with ground and aerial phenotyping platforms to carry out the analysis of crop phenotyping traits.

Potential crop phenotyping trait applications have been scored based on the difficulty of the data acquisition and the available optical sensors (Table 1). The results show that the highest and lowest potential crop phenotyping application levels are canopy coverage and plant diseases and pests, respectively. The high potential-application level of crop phenotyping traits includes canopy coverage, GAI, plant density, staygreen/senescence, canopy height, ear density, weed infestation, biomass, lodging, yield, water content, chlorophyll content, nitrogen content, FAPAR, monitoring of crop dynamics, phenology (e.g., anthesis), canopy temperature, leaf rolling, leaf angle, leaf wilting, nitrogen use efficiency, nitrogen nutrition index, grain number and size, canopy structure, chlorophyll fluorescence, photosynthetic status, grain quality, light use efficiency, water use efficiency, and plant diseases and pests. These potential application levels of crop phenotyping traits can provide a guideline for prioritizing trait selection using high-throughput methods at the field scale.

Figure 2 demonstrates potential applications of key crop phenotyping traits with different sensors at the critical growth stages in a maize breeding program. The figure presents the phenological stages of maize, including emergence (VE, 1), the first leaf collar (V1, 2), the third leaf collar (V3, 3), the sixth leaf collar (V6, 4), the ninth leaf collar (V9, 5), tasseling (VT, 6), silking (R1, 7), and maturity (R6, 8). An RGB camera is used to estimate the plant density in VE (1), the tassel density in VT (6), and the yield component in R6 (8) through color and texture information and related image-processing algorithms [39], [55], [74], respectively. The dynamic monitoring period of RGB cameras extends from the V1 (2) to the R6 (8) growth stages. Crop growth, diseases, stress, senescence, structure, phenology, and so on can be dynamically monitored by RGB cameras.

The key dynamic monitoring traits obtained by an RGB camera include GAI, FAPAR, height, anthesis, chlorophyll and nitrogen content, leaf rolling and angle, canopy coverage and structure, yield, and lodging. The dynamic monitoring stage of a multi/hyperspectral camera is consistent with that of an RGB camera, but key dynamic monitoring traits differ between the devices. For example, multi/hyperspectral cameras can be used to detect crop water content [116], [266] and grain quality [64], [274] through spectral characteristics and machine learning methods, with the exception of the same key dynamic monitoring traits from an RGB camera. The dynamic monitoring stage (3–8) of a thermal camera is less than that (2–8) of RGB and multi/hyperspectral cameras because thermal cameras' image resolution is not very high and plants are small at the V1 (2) stage [131]. Thermal cameras are mainly used to dynamically monitor crop growth, diseases, stress, temperature, and so on. The spectral region of a thermal camera [116], [131], [132], [271] enables the estimation of canopy temperature, leaf wilting, water content, lodging, leaf rolling, and water use efficiency.

There is a good consistency between the dynamic monitoring stage (3–8) and key dynamic monitoring traits of photosynthesis sensors and the dynamic monitoring stage (3–8) and key dynamic monitoring traits of fluorescence sensors. However, a photosynthesis sensor is specifically used to assess the photosynthetic status [159], and a fluorescence sensor is employed for evaluating the chlorophyll fluorescence [152]. The dynamic monitoring stage of a stereo camera is from V3 (3) to R1 (7). Due to their advantage of providing 3D structure images [130], stereo cameras can be used to monitor crop growth and structure, and their corresponding key dynamic monitoring traits involve height, leaf angle, lodging, leaf rolling, biomass, canopy coverage and structure, and yield. The dynamic monitoring stage (2–7) of lidar is longer than that of a stereo camera because lidar provides refined point cloud data that are used to describe small plants without the effect of illumination conditions [112]. The key dynamic monitoring traits of lidar agree with those of stereo cameras.

Figure 2 conveys a simple example of how to use different optical sensors to estimate key crop phenotyping traits across the growth stages in a maize breeding program; additional significant crop phenotyping traits are included in Table 2. Furthermore, different sensors can be comprehensively combined to improve the estimation accuracy of some vital phenotyping traits (such as lodging [134], yield [235], biomass [107], and so forth). More details are presented in the "Application of Ground and Aerial Phenotyping Platforms" section. In addition, a SPAD-502 chlorophyll meter [233] (a leaf-level sensor), an ultrasonic sensor [111], and the GreenSeeker system (a near-canopy sensor) [66] may be used, relatively inexpensively, to obtain the chlorophyll content, nitrogen content, and plant height, respectively.

Currently, it is a challenge to sufficiently improve the estimation accuracy of crop phenotyping traits with different optical sensors to satisfy the needs of crop

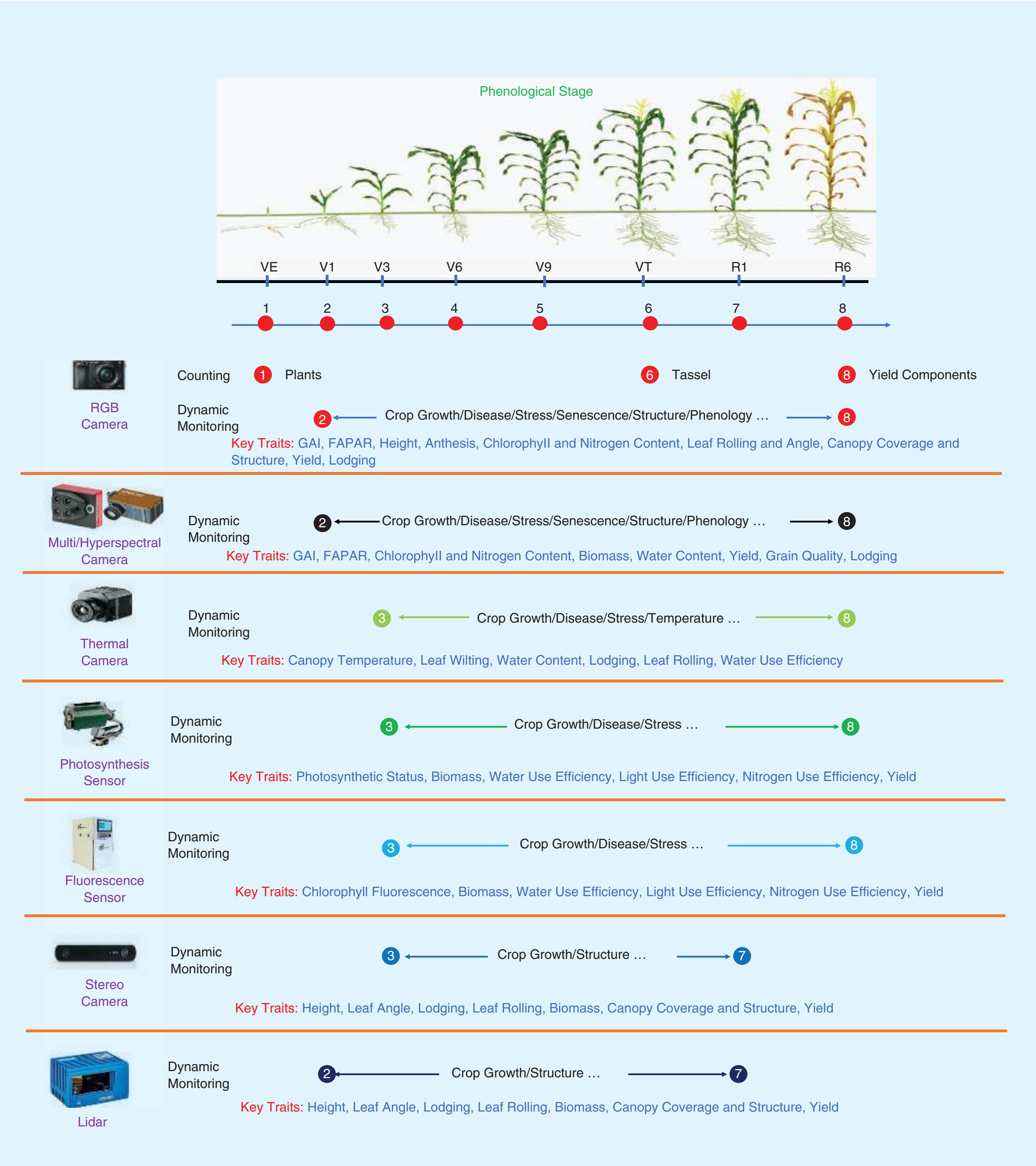


**FIGURE 2.** Examples of potential applications of field crop phenotyping with different sensors at the key growth stages in maize breeding programs. VE: emergence 1; V1: first leaf collar, 2; V3: third leaf collar, 3; V6: sixth leaf collar, 4; V9: ninth leaf collar, 5; VT: tasseling, 6; R1: silking, 7; R6: maturity, 8.

breeding programs [7]. There is a need for new ways to combine image information from different optical sensors (sensor fusion) to increase the estimation accuracy of crop phenotyping traits in the future. Image-processing scientists will increasingly focus in this direction to enhance the functionality of sensors in crop phenotyping studies [115].

## DEVELOPMENT OF GROUND AND AERIAL PHENOTYPING PLATFORMS AND APPLICATIONS

In this article, field phenotyping platforms are divided into two types based on ground and aerial levels. Currently, ground and aerial phenotyping platforms can carry different sensors to obtain crop phenotyping traits in the field. The ground and aerial phenotyping platforms are shown in detail in the next section and the "Aerial Phenotyping Platforms" section, respectively.

### GROUND PHENOTYPING PLATFORMS

Ground phenotyping platforms may be classified as phenopoles, phenomobiles, and stationary platforms (Figure 3). With phenopoles, poles (typically made from aluminum, steel, or plastic fibers) are used to directly mount sensors to obtain crop phenotyping trait data. Phenopoles include fixed and mobile versions. Fixed phenopoles are very similar to a field weather station: a low-cost RGB camera sensor is installed on a pole to obtain images that are updated to a server, for example, every 30 or 60 min based on sunlight illumination conditions [5]. The PhenoCam is an example of a fixed phenopole. The advantage of fixed phenopoles relates to the ability to obtain RGB images to monitor the dynamic changes to crops' canopy coverage, FAPAR, and GAI. The PhenoCam Network [275] uses digital cameras to track the seasonal dynamics of vegetation across a range of ecosystem types. Phenopoles are limited in that they focus only on a subsection of an experimental plot, and the price of a phenotyping study is expensive when cameras are installed across a large experimental site [59].

Mobile phenopoles are manually carried. Their camera is commonly controlled by a cellphone through Wi-Fi data transformation. Mobile phenopoles offer the advantage of obtaining higher-resolution images because they are near the ground level (1–3 m). Their limitation is that they require a lot of manpower to gather images for all the plots at a phenotyping experiment site. Fixed and mobile phenopoles are mainly used to obtain information pertaining to the plant density, canopy cover, GAI, flowering stage, VI, phenology, ear density, and so forth.

Phenomobiles include automatic, human, and tractor-propelled platforms. The automatic phenomobile commonly includes sensors, an integrated GPS system, a navigation control system, a data acquisition system, and a power supply [276]. The sensors and the integrated GPS system provide compatibility and efficient data acquisition, and they ensure that sensor outputs are recorded with navigation coordinates. The navigation control system is used to design a reasonable walking route through the field, while the data acquisition system maintains the consistency of the flashlight and monitors the obtained information to protect the data quality and minimize the effects of the background illumination. The power supply system

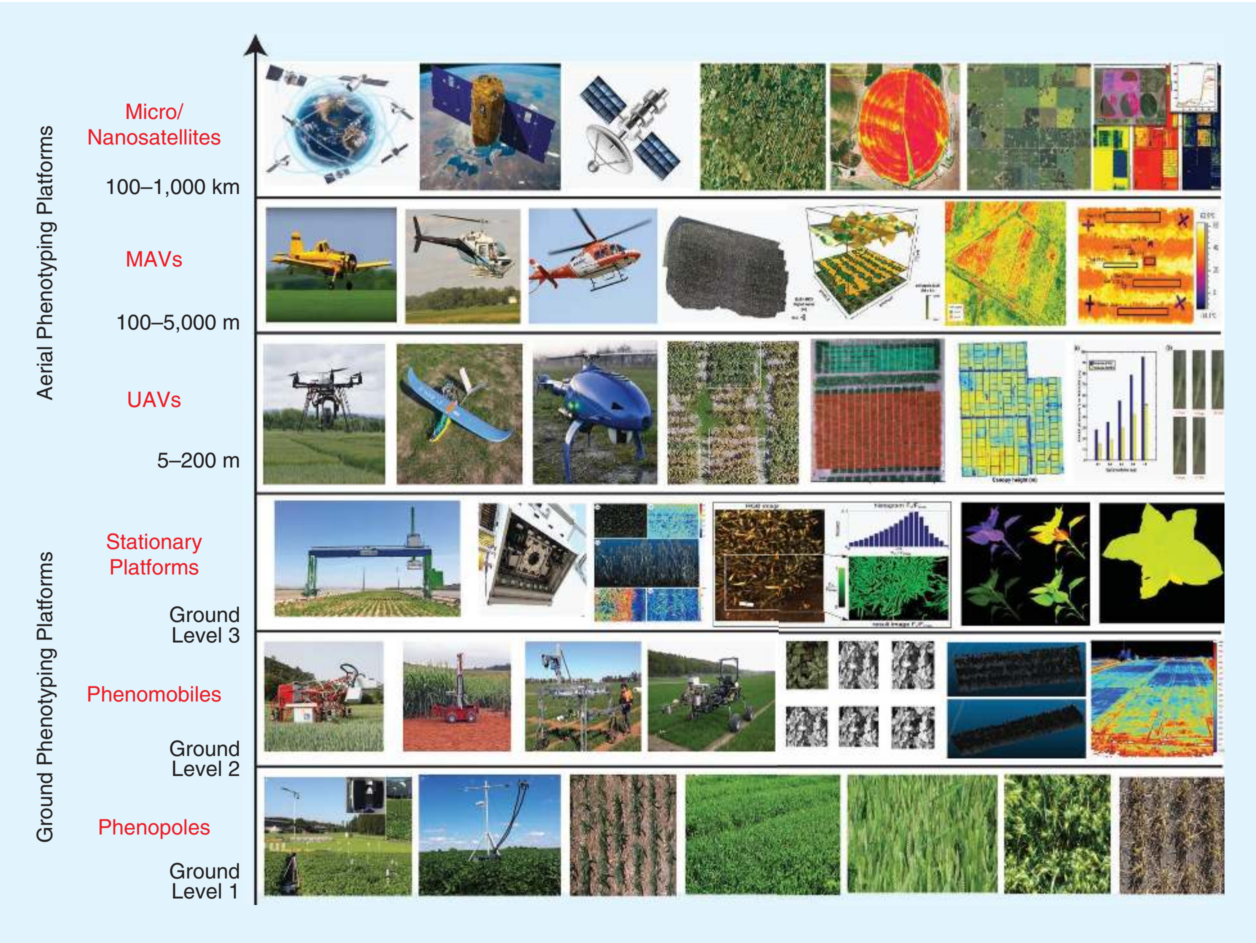


**FIGURE 3.** Ground phenotyping platforms (including stationary platforms, phenomobiles, and phenopoles) and aerial phenotyping platforms [including UAVs, manned aerial vehicles (MAVs), and micro/nanosatellites) [39], [40], [111], [200], [259], [260], [276], [280].

guarantees continuous electricity through a regulator. The cooperation between each system can safeguard the normal operation of the automatic phenomobile.

Currently, the automatic phenomobile can autonomously obtain RGB, multi/hyperspectral, and thermal images and point clouds using different optical sensors for each plot in a field. These images and point clouds can be employed to estimate the canopy cover, GAI, canopy height and temperature, chlorophyll and nitrogen content, water content, yield, grain quality, relative values of the in-season biomass, and so forth. The dynamic changes of crop phenotyping traits can be monitored through the automatic phenomobile without much human intervention. The advantage of the automatic phenomobile lies in the ability to simultaneously collect different types of images; however, such platforms are expensive. Current automatic phenomobile examples include Ladybird [277] at the University of Sydney, Australia, and Phenomobile [276] at the Institut National de la Recherche Agronomique, Paris, France.

Human phenomobiles are moved by manpower through a field. Examples include Phenomobile Lite [200], which contains data acquisition systems controlled by a person with a laptop. The system can incorporate RGB, multi/hyperspectral, and thermal sensors to obtain the related crop phenotyping traits. The price of human phenomobiles is low, but the data acquisition quality and efficiency of the sensors cannot be guaranteed.

Tractor phenomobiles consist of integrated sensor and GPS systems, a data acquisition system, and a power supply [278]. The basic integrated-sensor-and-GPS system combines non-image-based sensors (such as GreenSeeker and CropCircle, which are hyperspectral), the the outputs of which are recorded with GPS coordinates; similarly, the data acquisition system maintains the brightness of the flashlight and the consistency of the sensor data to ensure the quality the gathered information. The tractor provides the power supply. The PhenoTrac4 could be used to obtain VIs, nitrogen uptake, biomass, and water status. Its price is lower than other phenomobiles because its sensors are non-image-based [278]. Phenomobiles are relatively flexible in terms of sensors.

Finally, the sensors of stationary platforms include RGB cameras, multi/hyperspectral cameras, and thermal cameras and laser sensors. Stationary platforms are simultaneous and fully automated, fixed-site phenotyping equipment [279]. They can carry sensors for the noninvasive estimation of crop growth, physiology, morphology, and health. Their advantage is that they can simultaneously monitor different crop traits, although only in a defined area of, for example, roughly 1 hectare, when they are mounted on trackways [279].

### AERIAL PHENOTYPING PLATFORMS

Aerial phenotyping platforms may be classified as MAVs, UAVs, and micro/nanosatellites (Figure 3). Recent advances in technology have promoted the development of UAVs, which have been transformed into crop phenotyping platforms that provide high-spatial-resolution images for crop phenotyping trait estimation in the field [259], [260]. They include fixed-wing and multirotor configurations. Fixed-wing UAVs have the advantages of fast flight, high flight efficiency, long endurance time, large payload capacity, and a high flight altitude. However, they have certain requirements for taking off and landing, they cannot hover, and they will cause blurred images because of their high-speed shooting [281]. Multirotor UAVs have a simple structure, the ability to hover, and modest requirements for taking off and landing, but they possess a slow flight speed, short endurance time, a low flight altitude, and small payload volume [281].

Sensor images from UAVs are processed using Agisoft Photoscan Professional (Version 1.2.2, Agisoft, Saint Petersburg, Russia). The overlap between images should be larger than 60% for the software to compute the position of the camera corresponding to every acquired image [39]. The software can automatically recognize targets applied as ground control points (GCPs) for the absolute geopositioning of the images, and it can precisely locate the objects' center on the images [39]. The specific processing is conducted as follows:

1) check the camera calibration and optimizing the parameters
2) align the photos
3) build dense point cloud
4) construct the mesh
5) create the texture
6) build digital elevation models (DEMs)
7) develop the orthomosaic
8) export the orthomosaic and the DEMs.

The lidar point cloud from UAVs can be processed by CloudCompare or by writing code as needed [112], [199]. Currently, UAVs can carry different sensors (RGB cameras, multi/hyperspectral cameras, thermal cameras, and lidar) to estimate different crop traits at varying spatial scales. Images from UAVs can be employed to estimate grain yield [99], canopy temperature [266] and NDVI [259], [282], plant height [108], [282], [283], biomass [162], GAI [109], lodging [134], plant density [39], fluorescence [266], and nitrogen status [36], mostly through proxies for plant traits. The advantage of UAVs concerns the relatively high-resolution images that are obtainable in a relatively short time; however, it is difficult to cover very large areas due to the vehicles' limited range and speed. The onboard sensors of MAVs are comparable with those of UAVs. MAVs can cover larger regions in a relatively short time, albeit with a lower image resolution, and they have a greater payload capability. Images from MAVs are mainly used to estimate the GAI, biomass, chlorophyll content, nitrogen content, plant height, and biomass [8].

Finally, micro/nanosatellites can provide data in several spectral bands (which are sensitive to the crop structure, leaf pigment, and water content), and they enable meter-level-resolution images for estimating crop phenotyping traits at a very large scale [24], [79], [87], [88], [144], [193], [236], [239]. Micro/nanosatellites include optical and synthetic aperture radar (SAR) satellites. Optical satellites include the *Worldview* series, *QuickBird*, *Ikonos*, *Geoeye-1*, *Satellite for Earth Observation* series, *RapidEye*, *Landsat* series, *Gaofen* series, and so on. SAR satellites include the *Environmental Satellite* (*ENVISAT*), *Radar Satellite* (*RADARSAT*), *TerraSAR-X*, *Sentinel-1*, *Advanced Land Observation Satellite–Phased Array Type L-band Synthetic Aperture Radar*, and so forth. Optical satellite images are processed (including radiometric calibration, atmospheric correction, and geometric correction) using ENVI 4.7 software [284].

The fast line-of-sight atmospheric analysis of the spectral-hypercubes module is employed to retrieve the land surface reflectance. The geometric correction of each image is based on the measured GPS GCPs. SAR satellite images are processed using polarimetric SAR (PolSAR) Pro v5 [24], including the following steps:

1) The DN is converted into the backscattering coefficients using look-up tables in the product file (radiometric calibration) [285].
2) A 5 × 5 boxcar filter is applied for screening and for the multilook to suppress speckle [286].
3) The filtered SAR images are applied to obtain a scattering matrix (S2) and then converted to a symmetrized 3 × 3 covariance matrix (C3) [287].
4) The SAR images are orthorectified using DEM simulation and registration [288].
5) Finally, the SAR images are rectified using GPS GCPs.

Optical satellites use the relative reflectance at certain spectral wavelengths to estimate crop phenotyping traits based on VIs, machine learning methods, weather data, environmental factors, and crop varieties [79], [193], [236], [289]. However, optical satellites have saturation problems for VIs and a reduction in their estimation accuracy at high plant densities [24]. Compared with optical satellites, SAR satellites have some advantages for estimating crop phenotyping traits at high plant densities because SAR sensors use longer wavelengths, can penetrate crop canopies, and are not influenced by the presence of clouds and haze [88], [242]. For example, the backscatter and polarimetric decompositions of PolSAR are very sensitive to crop morphological structure changes [87]. SAR satellites have also been used to monitor crop phenology, yield, lodging, and so on through machine learning methods and polarimetric parameters [87], [143], [242]. More detail about the application of aerial phenotyping platforms is provided in the "Application of Ground and Aerial Phenotyping Platforms" section.

With the rapid development of micro/nanosatellite technology, higher-resolution images (<1 m) may be expected in the future. The advantages of micro/nanosatellites include international standard protocols for image processing at a relatively low cost. However, the image quality of micro/nanosatellites may be influenced by weather conditions, and the current resolution of micro/nanosatellites limits their application in crop trial monitoring [59]. A future possible application of images from micro/nanosatellites could lie in evaluating and verifying variety releases across wide geographic areas.

In summary, higher-resolution images are obtained by ground phenotyping platforms that have a relatively low efficiency in terms of coverage. Compared with ground phenotyping platforms, aerial phenotyping platforms can provide images with relatively high efficiency and cover larger areas. It is currently challenging to manage and process the images from ground phenotyping platforms; additionally, there are no international standards for doing so. Although image analysis protocols are available for UAVs and MAVs, large differences exist among laboratories. Scientists need to coordinate to develop internationally uniform protocols for image management and processing for ground and aerial phenotyping platforms, similar to the standard conventions for micro/nanosatellites.

## *APPLICATION OF GROUND AND AERIAL PHENOTYPING PLATFORMS*

This section introduces applications of ground and aerial phenotyping platforms for estimating crop phenotyping traits under different environmental conditions. Applications include early season crop mapping, crop growth condition monitoring (nitrogen stress, water stress, disease, phenological parameters, lodging, and others), and crop yield estimation.

### EARLY SEASON CROP MAPPING

Early and timely knowledge of crop types and conditions is extremely valuable information about regional production, yield estimation, and food security [290], [291]. Passive optical satellite sensors have been widely used for early season crop mapping because they improve the spectral, spatial, and temporal resolution of images and increase the availability of satellite data [292], [293]. In multitemporal remote sensing data, different classification algorithms have been used to process and analyze the time series of VIs to characterize growth conditions and then classify crop types during the early season [294]–[299]. Until now, several remote sensing classification algorithms have been successfully applied, such as support vector machines, random forest (RF), decision trees, and neural networks [300], [301]. Skakun et al. [302] used moderate-resolution imaging spectroradiometer (MODIS) NDVI data, a Gaussian mixture model, and growing-degree-days information to detect early season winter crops in large regions; the results showed a good consistency between official statistics and estimates ($R^2 = 0.85$).

In addition, SAR sensors can be used to classify crop types because they are not affected by clouds and atmospheric conditions [24]. Some scientists have investigated the potential of SAR backscatter data for crop mapping using images obtained by *Sentinel-1*, *RADARSAT-1* and 2, *ENVISAT* advanced SAR, and phased-array-type L-band SAR [303]–[308]. In recent years, some studies have carried out early season crop (wheat, cotton, spring maize, sugarcane, and rice) type classification based on the combination of optical satellite and SAR data [302], [307]–[309]. Hao et al. [307] used the improved artificial immune network and *Sentinel* data to carry out early season crop mapping in Hengshui, China, and the result indicated that the overall accuracy for summer crops and winter wheat was 98.55 and 99%, respectively. Jiang et al. [308] combined machine learning algorithms and *Sentinel-1A/2* time series data to map sugarcane during the early season in Zhanjiang City, China, and the outcome showed that the value of the kappa coefficient was 0.902 and that the estimation accuracy of the sugarcane mapping area was approximately 86.3%.

Compared with satellite platforms, UAVs can provide ultrahigh spatial resolution for classifying crops during the early season. UAVs equipped with RGB and multispectral cameras have been employed to classify weeds and crops [41], [311]. Zheng et al. [311] used RGB, NIR-G-B, and multispectral images from UAVs to detect rice plants during the early season, and the results indicated that a spectral-features decision tree had a high classification accuracy during the early growth stages. With the improvement of the spatial and temporal resolution of images from satellites and UAVs, deep-learning algorithms, e.g., convolutional neural networks (CNNs) [312] and recurrent neural networks [313], will ideally be employed to map early season crop types, with their advantages for image processing and analysis.

## CROP GROWTH CONDITION MONITORING

### NITROGEN STRESS

Nitrogen deficiency in crops results in a decreased chlorophyll content, a slower growth rate, and less photosynthesis as well as more sensitivity to diseases and pests [314]. These changes in the chlorophyll content, growth rate, photosynthesis, and disease and pest occurrence can be monitored using near-infrared and visible spectral reflectance [8], [29], [34]–[36]. These factors have been estimated using UAVs to monitor different nitrogen levels. The results demonstrated that multispectral and hyperspectral images from UAVs can estimate the biomass, nitrogen content, and grain yield with multiple nitrogen treatments [34]–[36]. In addition, a study by Camino et al. [35] showed that solar-induced chlorophyll fluorescence derived from hyperspectral images is a good indicator of photosynthesis under multiple nitrogen treatments in crop phenotyping experiments. Similarly, multispectral and hyperspectral sensors are integrated with phenomobiles to estimate the nitrogen content under different nitrogen treatments [67], [278]. Additionally, fluorescence sensors combined with UAVs and phenomobiles have a great potential for the early monitoring of crop traits under nitrogen stress in the field. Developing specific, lightweight spectral fluorescence sensors in combination with UAVs and phenomobiles for the early detection of nitrogen stress is a great opportunity.

### WATER STRESS

Stomata are typically closed under water-stressed conditions, which reduces crop growth and photosynthesis and may aggravate crop heat stress because of decreased transpirational cooling [8]. The canopy temperature is a good indicator of the response of crops to water stress [315], and scientists have reported that under water stress the measurement can be used to identify drought-adapted cultivars [114], [123], [136], [268], [316]–[318]. Thermal images need to be normalized to the ambient temperature and relative humidity to control the effect of environmental conditions on measurements. In a study, Jones et al. [268] indicated that the relative value among genotypes was more important than the absolute value for crop phenotyping evaluations. In addition, the background temperature (soil and dead leaves) of thermal images ideally should be eliminated from the signal of the green leaves using related image-segmentation algorithms [121].

Using thermal cameras with UAVs and phenomobile platforms enables the collection of more crop temperature images in less time compared to ground-based approaches [259], and it may assist in selecting water-stress-resistant genotypes. The limitation of the crop growth status (such as the biomass) owing to water stress could be estimated using near-infrared and visible optical sensors [319]. Therefore, hyperspectral and multispectral cameras can be applied in combination with thermal cameras to select water-stress-resistant genotypes [66], [123]. Images from thermal, multispectral, and hyperspectral cameras collected through the whole crop growing season can offer important quantitative and qualitative data sets that could be correlated with other ground-truthing data sets. These methods will promote the uptake of high-throughput, nondestructive sensors for estimating crop phenotyping traits in the field and may finally take the place of traditional data collection methods.

### DISEASES

Crop yield losses are persistent problems in agriculture due to the widespread occurrence of pathogens, such as fungi, viruses, nematodes, and bacteria. Advanced disease-monitoring technologies are required to minimize crop yield losses [98]. Remote sensing technologies have been applied to estimate diseases [320] and monitor new outbreaks worldwide [265]. However, the application of UAV-based optical sensors for detecting crop diseases and the tolerance of different crop varieties to maladies is less well developed [8], [99]. Nebiker et al. [99] used a threshold of NDVI values from multispectral images to identify blight infestation in potatoes. Crop diseases are mainly detected using near-ground optical sensors (such as hyperspectral, RGB, and thermal cameras) [100], [103], [104]. Recent research on detecting Huanglongbing (HLB) disease-infected citrus trees demonstrated that a good classification accuracy of HLB disease was obtained using the combination of visible, near infrared, and thermal spectral bands [100].

The results obtained by Jansen et al. [321] showed that a Cercospora leaf-spot index obtained from spectral indices was correlated with the Cercospora disease severity in sugar beet varieties. Furthermore, the classification accuracy of tomato diseases was better using a superresolution method (which produced a spatial resolution-enhanced image using low-resolution images) compared to using the conventional image-scaling methods with RGB images [103]. Behmann et al. [104] employed a miniaturized, handheld hyperspectral camera to identify powdery mildew at the canopy scale in barley. In short, these results indicated that the occurrence of disease and the resistance of crop varieties to infection can be effectively estimated using near-ground and UAV-based sensors. The fluorescence sensor was more sensitive to crop diseases than other instruments. It has the potential to be used in combination with hyperspectral, multispectral, RGB, and thermal cameras for the early detection of crop disease severity. Such sensors have a great potential to be harnessed to estimate the crop disease severity in future crop breeding programs. These near-ground and UAV-based sensors will detect the resistance of crop varieties to disease more effectively when combined with newly developed image classification methods.

### PHENOLOGICAL PARAMETERS

Crop phenology provides important information for simulating and monitoring crop growth and development [322], estimating crop yields [323], optimizing production management and decision-making [324], and analyzing crops' response to climate change [289]. Remote sensing-based observations with short revisit times and large spatial coverage have been employed to successfully retrieve crop phenological parameters using VI time-series data at regional to global scales [76], [77]. The NDVI and enhanced VI have been commonly employed to estimate crop phenology. The most-studied phenological parameters contain the start of season (SOS), peak of season, and end of season (EOS) [78]. Currently, various methods have been used to extract these phenological parameters using VI time series data, including dynamic threshold methods [79], fixed threshold methods [79], maximum-slope methods [80], function-fitting methods [81], moving average methods [82], and the valley-detection method [83].

The dynamic threshold method is the most commonly employed for estimating the crop SOS and EOS because it needs fewer parameters, has an easier application, and produces high-accuracy results. Sakamoto [84] developed the shaped model-fitting method with MODIS wide-dynamic-range VI time-series data to evaluate the timing of phenological parameters for 36 crop development stages of major U.S. food products. However, Verger et al. [85] found that leaf area index (LAI) is more robust and sensitive than VIs in considering vegetation from different satellite data. Furthermore, Luo et al. [86] used global land surface satellite LAI products and optimal filter-based phenology detection methods to obtain the crop SOS and EOS and produced a 1-km spatial resolution phenological survey of three staple crops in China from 2000 to 2015.

PolSAR is very sensitive to crop morphological structure changes [87]. *RADARSAT-2* and *TerraSAR-X* provide opportunities to explore the potential of these data for crop SOS and EOS estimation. Lopez-Sanchez et al. [88] used dual-polarized *TerraSAR-X* data and simple decision tree algorithms to evaluate rice phenological parameters. Furthermore, they harnessed the three polarimetric parameters (entropy, anisotropy, and alpha angle) from polarimetric *RADARSAT-2* data and hierarchical decision trees to estimate rice phenological parameters [89]. Wang et al. [87] applied the multitemporal *RADARSAT-2* dataset, SAR polarimetric decompositions, and an RF algorithm to monitor canola, maize, soybean, and wheat phenology based on crop phenological parameters. With the fast development of UAVs and sensors, near-real-time crop phenology retrieval is feasible. Yang et al. [90] proposed a near-real-time deep-learning method for monitoring rice phenological parameters and estimated rice phenology from UAV RGB images with an accuracy rate of 83.9%. In the future, the PhenoCams network will be combined with satellite images to better estimate different crops' phenological parameters. UAV images and advanced machine learning algorithms will improve crop phenological parameter retrieval in near real time and thus enable optimized crop management.

### LODGING

Crop lodging is the permanent deviation of crop plants from the upright position [325]. Crop lodging not only influences harvest operations but also results in yield losses and can reduce quality [326]. Therefore, accurate and rapid evaluation of crop lodging is important for research and screening, optimizing field crop management, obtaining better production, and estimating crop yield losses. The reflectance and backscatter at different wavelengths are affected by changes in the crop structure [327], biochemical properties [328], and morphology [329] in the lodging condition.

Many researchers have used crop phenotyping platforms to estimate crop lodging [134]–[143]. An early study by Fitch et al. [330] applied the linear polarization of backscatter from wheat to evaluate its potential in detecting wheat lodging using ground-based platforms. Ogden et al. [135] used motor-driven cameras to analyze textural information in images to estimate the extent of rice lodging. Liu et al. [331] demonstrated that optical hyperspectral data can be used to detect rice lodging. Recent advances in the development of UAVs and sensors have been used to detect crop lodging areas and evaluate lodging severity [134], [136]–[138]. Chapman et al. [136] reported that wheat lodging areas are successfully detected using thermal images from UAV-mounted thermal cameras. The combination of spectral and texture features and the digital surface model further increased the estimation accuracy of rice lodging classification using single-feature probability algorithms. In a recent study, Liu et al. [134] employed the fusion of RGB and thermal image information to improve the estimation accuracy of lodging classification in different rice species.

Satellite-based platforms can monitor crop lodging due to the availability of their images. Yang et al. [143] presented the potential of radar-based satellite images to detect wheat lodging at the farm scale, due to the sensitivity of SAR to crop structural changes. Some studies have employed *RADARSAT-2* quad-polarimetric images to estimate lodging in wheat and canola [142], [144]. In the future, the different phenotyping platforms and new machine learning algorithms will be better integrated to address the reasons for crop lodging and provide improved estimates of lodging at regional to global scales.

### *OTHER APPLICATIONS*

The different sensors from ground and aerial phenotyping platforms can be used to estimate many other important crop morphology phenotyping traits (GAI, canopy coverage, plant vigor, canopy height, leaf rolling, leaf angle, FAPAR, leaf staygreen/senescence, phenology, crop dynamics monitoring, biomass, and canopy structure), resource use phenotyping traits (nitrogen use efficiency, light use efficiency, and water use efficiency), yield component phenotyping traits (plant density, ear density, grain number and size, and grain quality), physiological phenotyping traits (chlorophyll content, water content, chlorophyll fluorescence, photosynthetic status, and nitrogen nutrition index), and stress phenotyping traits (plant diseases and pests and weed infestation) in crop breeding programs. In addition, the effects of soil components and compaction, field management practices, and soil spatial variability on crop phenotyping traits should be measured in parallel to include the effect of these environmental factors on the estimation accuracy of crop phenotyping traits.

### CROP YIELD ESTIMATION

Crop yield is widely used to measure cropland productivity. Estimating how much crop yield is obtained prior to harvesting is essential for field crop management, food trade balance, food security evaluation, and policy-making in the world [241], [332]. Furthermore, the rapid and efficient estimation of crop yield with high accuracy will allow identification of high-yielding genotypes in large germplasm panels [333]. Many studies have been successfully employed to estimate crop yield using different crop phenotyping platforms [170], [234]–[241], such as ground-based, UAV, and satellite-based platforms. For ground-based platforms, Jin et al. [170] assimilated the biomass and canopy cover derived from field hyperspectral VIs into the AquaCrop model based on the particle swarm optimization algorithm to improve the estimation accuracy of the maize yield with $R^2$ and root-mean-square error (RMSE) values of 0.78 and 1.44 tons/hectare, respectively. Li et al. [240] combined field spectral VIs and meteorological data through hierarchical linear modeling (HLM) to estimate wheat yield, and their results showed that the approximated power of yield estimation derived through HLM was higher than that obtained using ordinary least-squares regression, with $R^2$ and RMSE values of 0.75 and 1.10 tons/hectare, respectively.

For UAV platforms, Maimaitijiang et al. [235] applied multimodal data fusion and deep-learning methods to estimate the soybean yield from UAV RGB, multispectral, and thermal images, and the results demonstrated that the highest estimation accuracy was obtained by a deep neural network with an $R^2$ and relative RMSE of 0.720 and 15.9%, respectively. Another study by Yang et al. [238] used deep CNNs to estimate rice yield at the ripening stage from UAV, RGB, and multispectral imaging data and demonstrated that CNNs perform better than VI-based models for rice yield estimation ($R^2 = 0.59$ and RMSE = 0.66 tons/hectare).

Zhang et al. [237] extracted excess green color features from UAV RGB images and built an estimation model for maize yield, and the corresponding mean absolute percentage error ranged from 6.2 to 15.1%. For satellite-based platforms, Sakamoto [234] incorporated MODIS VIs and environmental variables to estimate the yields for maize and soybeans using a RF regression algorithm, and their results indicated that the RF method obtained a better yield estimation accuracy (maize RMSE = 0.539 ton/hectare and soybean RMSE = 0.206 ton/hectare) at the state level. Similarly, Schwalbert et al. [236] integrated long short-term memory (LSTM) neural networks, weather data, and machine learning for improving crop yield prediction in southern Brazil and showed that LSTM neural networks performed better than other algorithms. In addition, Dong et al. [145] estimated wheat yield using a light use efficiency model and wheat variety data, and the results indicated that the proposed method enhanced the model simulation performance and achieved an 82% estimation accuracy of the interannual yield variation.

In short, the preceding studies demonstrated that the combination of different crop phenotyping platform images, meteorological data, crop models, variety data, environmental variables, and machine learning methods could be used improve current estimation accuracy of crop yield. In particular, deep-learning algorithms, such as deep CNNs and LSTM neural networks, can significantly improve the estimation accuracy of crop yield. It can be assumed that researchers will have to pay more attention to the integration of multisource data with deep-learning methods to improve crop yield estimation in the future.

## FUTURE PERSPECTIVES

While high-throughput crop phenotyping technologies have made some progress, further improvements are needed due to the requirements for more accurate estimations of most crop phenotyping traits. Advanced sensors, together with cutting-edge ground and aerial phenotyping platforms, have led to a major requirement for advances in image processing. Recently, new machine learning algorithms have been used to identify useful crop traits using image information. For example, deep-learning algorithms have shown advantages for trait detection and segmentation [46], [103]. Crop phenotyping sensors are commonly influenced by field environmental conditions; therefore, developments of more stable and refined crop phenotyping sensors are necessary for field crop phenotyping research.

Currently, many crop phenotyping sensors and platforms are too expensive for numerous crop breeding programs; however, the rapid development of miniaturized and mobile technologies has provided some affordable and powerful sensors for crop phenotyping with high-resolution images. As sensors have become lighter and smaller, they have been integrated with the different ground and aerial phenotyping platforms, facilitating crop phenotyping research [59], [115], [281]. RGB, multispectral, hyperspectral, and thermal cameras; photosynthesis and fluorescence sensors; stereo cameras; and lidar have been used to evaluate crop phenotyping traits. How to combine the outputs of these sensors to increase the estimation accuracy of crop phenotyping traits is still a challenge for crop phenotyping traits [7], [59]. Micro/nanosatellites with relatively high-resolution images also provide a good resource for crop phenotyping traits in large-scale validation, due, in part, to the international standard protocols for image processing.

The combination of available sensors and platforms provides ground-based crop phenotyping platform systems with the ability to simultaneously obtain, process, and store data in an affordable and efficient manner [59]. However, compatibility issues between software and hardware still exist. In addition, the processing of images from ground-based crop phenotyping platform systems does not have internationally uniform standards, so the use and sharing of image data sets will be limited [14]. Multidisciplinary teams are needed to build efficient integrated crop phenotyping management systems. Such systems need user-friendly data analysis and management interfaces that are integrated with data selection and processing and decision-making functions.

Furthermore, corresponding field soil properties and weather information should be included with image data set analyses and management systems to increase the estimation accuracy and stability of crop phenotyping traits [59]. Finally and importantly, the rapid development of high-throughput crop phenotyping technology will improve future study of precision agriculture. How to effectively combine these crop phenotyping traits and agronomic indicators to enhance crop field management at different growth stages, and thus implement precision agriculture, will be a long-term goal [243].

In summary, crop phenotyping platforms should be adopted by crop breeders as a powerful tool for genetic improvement. It is against this background that affordable and efficient crop phenotyping systems will become the routine choice for crop breeding programs. A crop functional structure model has been used to simulate crop 3D growth structural changes during the whole crop growth season. This can be integrated with crop phenotyping platforms to improve the estimation accuracy of crop phenotypic traits using data assimilation methods, and it can be used to design crop ideotypes for the future.

However, in many cases, this kind of information would be more detailed than most breeders need. Their main requirements would be reliable estimates of the heading date and plant height, spectral indices that detect biotic and abiotic stress, and approximations of the yield and yield components, including spike density and biomass [310]. These traits can generally be remotely projected with sufficient heritability and combined into selection indices to help choose material that is either for advancement to the next breeding generation or for inclusion in multilocation trials. In addition, QTL and GWAS approaches are not always successful for analyzing relationships between genetics and phenotype and then selecting key gene loci [5]. Therefore, the QTL and GWAS approaches will need to be improved by combing other statistical methods (such as meta-analysis, meta-GWAS methods, and so forth) to identify more stable and effective key gene loci in the future.

## CONCLUSION

High-throughput crop phenotyping trait selection is important for improving crop yield and stress resistance under different biotic/abiotic environmental conditions in plant breeding programs. Currently, the ability to provide high-throughput identification of crop phenotyping traits limits our capacity to determine quantitative genetic traits linked with yields, crop growth statuses, and adaptation to environmental stress. The rapid development of sensors, ground and aerial phenotyping platforms, and image-processing technologies is providing effective tools for high-throughput crop phenotyping traits in field.

This article first introduced the origin and definition of crop phenotyping. Second, it described the development of current sensors (RGB, multispectral, hyperspectral, and thermal cameras; photosynthesis and fluorescence sensors; stereo cameras; and lidar) for crop phenotyping traits in the field, including an analysis of the advantages and limitations of different sensors and their levels of potential application. Third, it highlighted the development of ground (stationary platforms, phenomobiles, and phenopoles) and aerial (UAVs, MAVs, and micro/nanosatellites) phenotyping platforms and their applications for crop phenotyping under nitrogen, water, and disease stresses in the field. Finally, new opportunities and directions of crop phenotyping technological developments for the future were presented. In the future, high-throughput crop phenotyping technology will increase the estimation accuracy of measuring standard crop traits and further accelerate the efficiency of new trait identification in crop breeding programs, based on newly developed sensors, phenotyping platforms, and image processing and data management methods.

## ACKNOWLEDGMENTS

The study was supported by the National Key Research and Development Program of China (grant 2016YFD0300605), National Natural Science Foundation of China (grant 41601369), and the Young Talents Program of the Institute of Crop Science under the Chinese Academy of Agricultural Sciences (grant S2019YC04). Malcolm J. Hawkesford is supported by the Biotechnology and Biological Sciences Research Council of the United Kingdom for funding the Designing Future Wheat program (grant BB/P016855/1) and the United Kingdom Department for Environment, Food, and Rural Affairs for funding the Wheat Genetic Improvement Network (grant CH1090).

## AUTHOR INFORMATION

**Xiuliang Jin** (jinxiuliang@caas.cn) received his B.S. degree in forestry from Shihezi University, China, in 2008; his M.S. degree in agronomy from Shihezi University in 2011; and his Ph.D. degree in agronomy from Yangzhou University, China, in 2015. He is a professor in and head of the Crop Phenotypic Innovation Research group, Institute of Crop Science, Chinese Academy of Agriculture Sciences. He mainly engages in crop phenotyping identification and agricultural remote sensing. Since 2011, as the first or corresponding author, he has published 25 Science Citation Index-listed papers, and he has coauthored more than 50. He is associate editor of *Journal of Agricultural Science* and *Agronomy Journal*, an editorial board member of *Scientific Reports* and *Crop Magazine*, and a guest editor of the *IEEE Geoscience and Remote Sensing Magazine* special issue "Estimation of Crop Phenotyping Traits Using Unmanned Ground Vehicle and Unmanned Aerial Vehicle Imagery."

**Pablo J. Zarco-Tejada** (pablo.zarco@unimelb.edu.au) received his B.Sc. degree in agricultural engineering from the University of Córdoba, Spain; his M.Sc. degree in remote sensing from the University of Dundee, United Kingdom; and his Ph.D. degree in Earth and space science from York University, Toronto. He is jointly appointed between the School of Agriculture and the Melbourne School of Engineering, University of Melbourne, Australia, and he is an honorary scientist at the Spanish National Research Council. As the leader of the HyperSens Laboratory, he focuses on remote sensing for biotic and abiotic stress detection using hyperspectral and thermal images acquired by manned and unmanned aircraft systems. A highly cited researcher in 2019, he is the author of more than 100 papers published in international journals. He is associate editor of *Remote Sensing of Environment* and *European Journal of Agronomy* and has received awards in Spain, the United Kingdom, and Canada.

**Urs Schmidhalter** (schmidhalter@wzw.tum.de) received his diploma degree in agronomy from ETH Zürich, Switzerland. He received his Ph.D. degree in technical sciences from ETH Zürich, where he worked as a postdoctoral research associate, principal investigator, and docent in plant nutrition, receiving a habilitation degree in 1996. He has been chair of plant nutrition at the Technical University of Munich since 1997. Previously, he was a research assistant in soil physics and soil chemistry at the Swiss Federal Research Station for Agronomy and a consulting engineer in agrohydrology and ecotoxicology. He participated in and led numerous national and international research projects, in addition to writing more than 200 research papers and 150 technical publications. He serves as an associate editor of *European Journal of Agronomy* and as topic editor of *Frontiers in Plant Science*.

**Matthew P. Reynolds** (m.reynolds@cgiar.org) received his B.A. degree in botany from Oxford University in 1983, his M.Sc. degree in agricultural botany from Reading University in 1984, and his Ph.D. degree in horticultural science from Cornell University in 1989. He is a distinguished scientist and head of wheat physiology at the International Maize and Wheat Improvement Center. He serves on the management committee of the Consultative Group for International Agricultural Research Platform for Big Data in Agriculture, for which he also leads the Community of Practice for Crop Modeling. He has honorary positions at the University of Nottingham, Texas A&M University, and Oklahoma State University, and he is a board member of the Global Plant Council. He has published more than 200 articles in peer-reviewed journals, including 13,000-plus citations and an H index of 62. He was included by Web of Science in the top 1% of the world's researchers in 2018 and 2019 across 21 fields.

**Malcolm J. Hawkesford** (malcolm.hawkesford@rothamsted.ac.uk) received his B.Sc. degree with honors in botany at Liverpool University, United Kingdom, in 1979 and his Ph.D. degree in nitrogen fixation in cyanobacteria at Dundee University, United Kingdom, in 1982. Since 1998, he has worked at Rothamsted Research, Harpenden, United Kingdom, where he is head of the Plant Sciences Department and leads the institute's contribution to the U.K. Designing Future Wheat strategic research program. He was a postdoctoral fellow at Brookhaven National Laboratory, Upton, New York, and the University of Edinburgh, Scotland, working in molecular mechanisms of energy transduction. From 1987 to 1998, he was a project leader in plant nutrition at Long Ashton Research Station, United Kingdom. He is an honorary professor in plant sciences in the School of Biosciences, University of Nottingham, United Kingdom. He has published widely on crop nutrition, from the field to underpinning molecular mechanisms and, most recently, within the area of crop phenotyping.

**Rajeev K. Varshney** (r.k.varshney@cgiar.org) received his B.S. degree in botany from Aligarh Muslim University, India, in 1993; his M.S. degree in botany from Aligarh Muslim University in 1995; and his Ph.D. degree in agricultural botany from Chaudhary Charan Singh University, Meerut, India, in 2001. He serves as the global research program director for genetic gains and the director of the Center of Excellence in Genomics and Systems Biology at

the International Crops Research Institute for the Semi-Arid Tropics, Hyderabad, India. He is an honorary or adjunct professor at 10 universities/institutes in Australia, China, Ghana, and India, including the University of Western Australia and the University of Queensland, Australia. He is an agricultural research scientist specializing in genomics and molecular breeding with 20-plus years service in developing countries in sub-Saharan Africa and Asia. He is a globally recognized leader for his work on genome sequencing, genomics-assisted breeding, and translational genomics in legume and cereal crops and capacity building in developing countries.

**Tao Yang** (yangtao02@caas.cn) received his B.S. degree in biological sciences from China Agricultural University, Beijing, in 2003 and his Ph.D. degree in botany from China Agricultural University in 2010. He works at the Center for Crop Germplasm Resources at the Institute of Crop Sciences, Chinese Academy of Agriculture Sciences. He has written more than 15 research papers as well as five books or book chapters, and he holds three patents. He is a member of the Crop Science Society of China.

**Chenwei Nie** (nie_chenwei@126.com) received his B.S. degree in electronic information engineering from the North China Institute of Aerospace Engineering, Langfang, in 2011; his M.S. degree in computer application technology from China Three Gorges University, Yichang, in 2014; and his Ph.D. degree in cartography and geography information systems from the Institute of Remote Sensing and Digital Earth, Chinese Academy of Sciences, Beijing, in 2019. He is a postdoctoral researcher in crop phenotypes at the Institute of Crop Science, Chinese Academy of Agricultural Sciences.

**Zhenhai Li** (lizh@nercita.org.cn) received his B.S. degree in agricultural science from Shandong Agricultural University, Tai'an, China, in 2011 and his Ph.D. degree in agriculture remote sensing and information technology from Zhejiang University, China, in 2016. He is a research associate in remote sensing at the National Engineering Research Center for Information Technology in Agriculture, Beijing. From January 2017 to August 2018, he worked as a research associate in the School of Engineering, Newcastle University, United Kingdom. He has more than 18 papers and one book to his credit and holds two patents. He is a member of Agronomy Modeling and Simulation Group of the Chinese Simulation Society.

**Bo Ming** (mingbo@caas.cn) received his B.S. degree in physics from Shandong Agriculture University, Tai'an, China, in 2005; his M.S. degree in agronomy from Shihezi University, China, in 2009; and his Ph.D. degree in agronomy from China Agriculture University, Beijing, in 2013. He is an assistant researcher on the Crop Cultivation and Physiological Innovation team at the Institute of Crop Sciences, Chinese Academy of Agricultural Sciences, Beijing. He has 38 research papers to his credit.

**Yonggui Xiao** (xiaoyonggui@caas.cn) received his B.S. degree in agronomy from Henan Agricultural University, Zhengzhou, China; his M.S. degree in plant breeding and genetics from Xinjiang Agricultural University, Urumqi, China; and his Ph.D. degree in physiological genetics and molecular biology from the Northwest Agriculture and Forestry University and the Chinese Academy of Agricultural Sciences, Beijing. He is an associate professor and wheat breeder at the Institute of Crop Sciences, Chinese Academy of Agricultural Sciences, Beijing. His research interests include wheat physiology, genetics, and variety improvement. His team is developing new molecular markers and phenotyping technologies for use in wheat associated with breeding. He focuses on developing field-based, high-throughput phenotyping technologies to accelerate applied genomics and breeding research.

**Yongdun Xie** (xieyongdun@caas.cn) received his B.S. degree in biotechnology from the Agricultural University of Hebei, China, in 2003, and his Ph.D. degree in biochemistry and molecular biology from the China Agricultural University, Beijing, in 2010. He is working on wheat breeding using combined approaches, including molecular biology, mutation induction, phenomics methods, and traditional techniques. He has published 14 papers and released four new wheat varieties.

**Shaokun Li** (lishaokun@caas.cn) received his B.S. degree in agronomy from Shihezi University, China, in 1984; his M.S. degree in agronomy from Shihezi University in 1990; and his Ph.D. degree in agronomy from the China Agriculture University, Beijing, in 1996. He leads the Crop Cultivation and Physiology Center for Crop Management and Farming Systems at the Institute of Crop Sciences, Chinese Academy of Agricultural Sciences, Beijing. He mainly engages in the physiology and ecology of maize yield formation, achieving high yields, and finding potential breakthroughs. He has published more than 200 research papers and 17 books. He was a recipient of the National Science and Technology Progress Award, National Innovation Pioneer Medal, and other recognitions. He is the executive editor of *Journal of Integrative Agriculture* and *Journal of Maize Science*.

## REFERENCES

[1] R. L. Phillips, "Mobilizing science to break yield barriers," *Crop Sci.*, vol. 50, no. S_1, pp. S-99–S-108, 2010. doi: 10.2135/cropsci2009.09.0525.

[2] S. Sukumaran, S. Dreisigacker, M. Lopes, P. Chavez, and M. P. Reynolds, "Genome-wide association study for grain yield and related traits in an elite spring wheat population grown in temperate irrigated environments," *Theor. Appl. Genet.*, vol. 128, no. 2, pp. 353–363, 2015. doi: 10.1007/s00122-014-2435-3.

[3] S. Sukumaran, M. P. Reynolds, and C. Sansaloni, "Genome-wide association analyses identify QTL hotspots for yield and component traits in durum wheat grown under yield potential, drought, and heat stress environments," *Front. Plant Sci.*, vol. 9, p. 81, Feb. 2018. doi: 10.3389/fpls.2018.00081.

[4] C. Xu et al., "Genome-wide association study dissects yield components associated with low-phosphorus stress tolerance

in maize," *Theor. Appl. Genet.*, vol. 131, no. 8, pp. 1699–1714, 2018. doi: 10.1007/s00122-018-3108-4.

[5] J. L. Araus, S. C. Kefauver, M. Zaman-Allah, M. S. Olsen, and J. E. Cairns, "Translating high-throughput phenotyping into genetic gain," *Trends Plant Sci.*, vol. 23, no. 5, pp. 451–466, 2018. doi: 10.1016/j.tplants.2018.02.001.

[6] R. T. Furbank and M. Tester, "Phenomics: Technologies to relieve the phenotyping bottleneck," *Trends Plant Sci.*, vol. 16, no. 12, pp. 635–644, 2011. doi: 10.1016/j.tplants.2011.09.005.

[7] J. L. Araus and J. E. Cairns, "Field high-throughput phenotyping: The new crop breeding frontier," *Trends Plant Sci.*, vol. 19, no. 1, pp. 52–61, 2014. doi: 10.1016/j.tplants.2013.09.008.

[8] S. Sankaran et al., "Low-altitude, high-resolution aerial imaging systems for row and field crop phenotyping: A review," *Eur. J. Agron.*, vol. 70, pp. 112–123, Oct. 2015. doi: 10.1016/j.eja.2015.07.004.

[9] J. Diamond and C. Renfrew, "Guns, germs, and steel: The fates of human societies," *Nature*, vol. 386, no. 6623, pp. 339–339, 1997.

[10] M. Mahner and M. Kary, "What exactly are genomes, genotypes and phenotypes? And what about phenomes?" *J. Theor. Biol.*, vol. 186, no. 1, pp. 55–63, 1997. doi: 10.1006/jtbi.1996.0335.

[11] F. Fiorani and U. Schurr, "Future scenarios for plant phenotyping," *Annu. Rev. Plant Biol.*, vol. 64, no. 1, pp. 267–291, 2013. doi: 10.1146/annurev-arplant-050312-120137.

[12] A. B. Gjuvsland, J. O. Vik, D. A. Beard, P. J. Hunter, and S. W. Omholt, "Bridging the genotype–phenotype gap: What does it take?" *J. Physiol.*, vol. 591, no. 8, pp. 2055–2066, 2013. doi: 10.1113/jphysiol.2012.248864.

[13] R. Pieruschka and H. Poorter, "Phenotyping plants: Genes, phenes and machines," *Funct. Plant Biol.*, vol. 39, no. 11, pp. 813–820, 2012. doi: 10.1071/FPv39n11_IN.

[14] D. Houle, D. R. Govindaraju, and S. Omholt, "Phenomics: The next challenge," *Nat. Rev. Genet.*, vol. 11, no. 12, pp. 855–866, 2010. doi: 10.1038/nrg2897.

[15] C. H. Pearson, S. M. Ernst, K. A. Barbarick, J. L. Hatfield, G. A. Peterson, and D. R. Buxton, "Agronomy Journal turns one hundred," *Agron. J.*, vol. 100, no. 1, pp. 1–8, 2008. doi: 10.2134/agrojnl2006.0312c.

[16] P. Annicchiarico, *Genotype X Environment Interactions: Challenges and Opportunities for Plant Breeding and Cultivar Recommendations (No. 174)*. Quebec City, PQ: Food & Agriculture Org., 2002.

[17] S. Jay, F. Maupas, R. Bendoula, and N. Gorretta, "Retrieving LAI, chlorophyll and nitrogen contents in sugar beet crops from multi-angular optical remote sensing: Comparison of vegetation indices and PROSAIL inversion for field phenotyping," *Field Crops Res.*, vol. 210, pp. 33–46, Aug. 2017. doi: 10.1016/j.fcr.2017.05.005.

[18] M. Maimaitijiang et al., "Unmanned Aerial System (UAS)-based phenotyping of soybean using multi-sensor data fusion and extreme learning machine," *ISPRS J. Photogramm. Remote Sens.*, vol. 134, pp. 43–58, Dec. 2017. doi: 10.1016/j.isprsjprs.2017.10.011.

[19] A. B. Potgieter et al., "Multi-spectral imaging from an unmanned aerial vehicle enables the assessment of seasonal leaf area dynamics of sorghum breeding lines," *Front. Plant Sci.*, vol. 8, p. 1532, Sept. 2017. doi: 10.3389/fpls.2017.01532.

[20] P. P. Roosjen, B. Brede, J. M. Suomalainen, H. M. Bartholomeus, L. Kooistra, and J. G. Clevers, "Improved estimation of leaf area index and leaf chlorophyll content of a potato crop using multi-angle spectral data: Potential of unmanned aerial vehicle imagery," *Int. J. Appl. Earth Observ. Geoinform.*, vol. 66, pp. 14–26, Apr. 2018. doi: 10.1016/j.jag.2017.10.012.

[21] A. Verger, N. Vigneau, C. Chéron, J.-M. Gilliot, A. Comar, and F. Baret, "Green area index from an unmanned aerial system over wheat and rapeseed crops," *Remote Sens. Environ.*, vol. 152, pp. 654–664, Sept. 2014. doi: 10.1016/j.rse.2014.06.006.

[22] M. Zaman-Allah et al., "Unmanned aerial platform-based multispectral imaging for field phenotyping of maize," *Plant Methods*, vol. 11, no. 1, p. 35, 2015. doi: 10.1186/s13007-015-0078-2.

[23] J. Yue et al., "A comparison of crop parameters estimation using images from UAV-mounted snapshot hyperspectral sensor and high-definition digital camera," *Remote Sens.*, vol. 10, no. 7, p. 1138, 2018. doi: 10.3390/rs10071138.

[24] X. Jin et al., "Combined multi-temporal optical and radar parameters for estimating LAI and biomass in winter wheat using HJ and RADARSAR-2 data," *Remote Sens.*, vol. 7, no. 10, pp. 13,251–13,272, 2015. doi: 10.3390/rs71013251.

[25] Z. Li et al., "Estimating winter wheat (*Triticum aestivum*) LAI and leaf chlorophyll content from canopy reflectance data by integrating agronomic prior knowledge with the PROSAIL model," *Int. J. Remote Sens.*, vol. 36, no. 10, pp. 2634–2653, 2015. doi: 10.1080/01431161.2015.1041176.

[26] X. Li et al., "Exploring the best hyperspectral features for LAI estimation using partial least squares regression," *Remote Sens.*, vol. 6, no. 7, pp. 6221–6241, 2014. doi: 10.3390/rs6076221.

[27] X.-l. Jin et al., "Estimation of wheat agronomic parameters using new spectral indices," *PLoS One*, vol. 8, no. 8, p. e72736, 2013. doi: 10.1371/journal.pone.0072736.

[28] A. Pask, J. Pietragalla, D. Mullan, and M. Reynolds, *Physiological Breeding II: A Field Guide to Wheat Phenotyping*. CIMMYT, Mexico City, 2012.

[29] M. Saberioon, M. Amin, A. Anuar, A. Gholizadeh, A. Wayayok, and S. Khairunniza-Bejo, "Assessment of rice leaf chlorophyll content using visible bands at different growth stages at both the leaf and canopy scale," *Int. J. Appl. Earth Observ. Geoinform.*, vol. 32, pp. 35–45, Oct. 2014. doi: 10.1016/j.jag.2014.03.018.

[30] J. Vollmann, H. Walter, T. Sato, and P. Schweiger, "Digital image analysis and chlorophyll metering for phenotyping the effects of nodulation in soybean," *Comput. Electron. Agric.*, vol. 75, no. 1, pp. 190–195, 2011. doi: 10.1016/j.compag.2010.11.003.

[31] J. P. Baresel et al., "Use of a digital camera as alternative method for non-destructive detection of the leaf chlorophyll content and the nitrogen nutrition status in wheat," *Comput. Electron. Agric.*, vol. 140, pp. 25–33, Aug. 2017. doi: 10.1016/j.compag.2017.05.032.

[32] X. Jin, Z. Li, H. Feng, X. Xu, and G. Yang, "Newly combined spectral indices to improve estimation of total leaf chlorophyll content in cotton," *IEEE J. Sel. Topics Appl. Earth Observ. Remote Sens.*, vol. 7, no. 11, pp. 4589–4600, 2014. doi: 10.1109/JSTARS.2014.2360069.

[33] X.-l. Jin et al., "Comparison of two methods for estimation of leaf total chlorophyll content using remote sensing in wheat,"

*Field Crops Res.*, vol. 135, pp. 24–29, Aug. 2012. doi: 10.1016/j.fcr.2012.06.017.

[34] J. Geipel, J. Link, J. A. Wirwahn, and W. Claupein, "A programmable aerial multispectral camera system for in-season crop biomass and nitrogen content estimation," *Agriculture*, vol. 6, no. 1, p. 4, 2016. doi: 10.3390/agriculture6010004.

[35] C. Camino, V. González-Dugo, P. Hernández, J. Sillero, and P. J. Zarco-Tejada, "Improved nitrogen retrievals with airborne-derived fluorescence and plant traits quantified from VNIR-SWIR hyperspectral imagery in the context of precision agriculture," *Int. J. Appl. Earth Observ. Geoinform.*, vol. 70, pp. 105–117, Aug. 2018. doi: 10.1016/j.jag.2018.04.013.

[36] H. Liu, H. Zhu, and P. Wang, "Quantitative modelling for leaf nitrogen content of winter wheat using UAV-based hyperspectral data," *Int. J. Remote Sens.*, vol. 38, no. 8–10, pp. 2117–2134, 2017. doi: 10.1080/01431161.2016.1253899.

[37] J.-J. Wang et al., "Phenotyping flag leaf nitrogen content in rice using a three-band spectral index," *Comput. Electron. Agric.*, vol. 162, pp. 475–481, July 2019. doi: 10.1016/j.compag.2019.04.042.

[38] Z. Li et al., "Remote sensing of leaf and canopy nitrogen status in winter wheat (*Triticum aestivum* L.) based on N-PROSAIL model," *Remote Sens.*, vol. 10, no. 9, p. 1463, 2018. doi: 10.3390/rs10091463.

[39] X. Jin, S. Liu, F. Baret, M. Hemerlé, and A. Comar, "Estimates of plant density of wheat crops at emergence from very low altitude UAV imagery," *Remote Sens. Environ.*, vol. 198, pp. 105–114, Sept. 2017. doi: 10.1016/j.rse.2017.06.007.

[40] S. Varela et al., "Early-season stand count determination in corn via integration of imagery from unmanned aerial systems (UAS) and supervised learning techniques," *Remote Sens.*, vol. 10, no. 3, p. 343, 2018. doi: 10.3390/rs10020343.

[41] D. Stroppiana et al., "Early season weed mapping in rice crops using multi-spectral UAV data," *Int. J. Remote Sens.*, vol. 39, no. 15–16, pp. 5432–5452, 2018. doi: 10.1080/01431161.2018.1441569.

[42] Z. Fan, J. Lu, M. Gong, H. Xie, and E. D. Goodman, "Automatic tobacco plant detection in UAV images via deep neural networks," *IEEE J. Sel. Topics Appl. Earth Observ. Remote Sens.*, vol. 11, no. 3, pp. 876–887, 2018. doi: 10.1109/JSTARS.2018.2793849.

[43] E. Hamuda, M. Glavin, and E. Jones, "A survey of image processing techniques for plant extraction and segmentation in the field," *Comput. Electron. Agric.*, vol. 125, pp. 184–199, July 2016. doi: 10.1016/j.compag.2016.04.024.

[44] R. Chen, T. Chu, J. A. Landivar, C. Yang, and M. M. Maeda, "Monitoring cotton (*Gossypium hirsutum* L.) germination using ultrahigh-resolution UAS images," *Precis. Agric.*, vol. 19, no. 1, pp. 161–177, 2018. doi: 10.1007/s11119-017-9508-7.

[45] L. Prey, M. von Bloh, and U. Schmidhalter, "Evaluating RGB imaging and multispectral active and hyperspectral passive sensing for assessing early plant vigor in winter wheat," *Sensors*, vol. 18, no. 9, p. 2931, 2018. doi: 10.3390/s18092931.

[46] S. Madec et al., "Ear density estimation from high resolution RGB imagery using deep learning technique," *Agric. For. Meteorol.*, vol. 264, pp. 225–234, 2019. doi: 10.1016/j.agrformet.2018.10.013.

[47] J. A. Fernandez-Gallego, S. C. Kefauver, N. A. Gutiérrez, M. T. Nieto-Taladriz, and J. L. Araus, "Wheat ear counting in-field conditions: High throughput and low-cost approach using RGB images," *Plant Methods*, vol. 14, no. 1, p. 22, 2018. doi: 10.1186/s13007-018-0289-4.

[48] L. Tao, S. Chengming, and W. Lijian, "In-field wheatear counting based on image processing technology," *Trans. Chin. Soc. Agric. Mach.*, vol. 45, no. 2, pp. 282–290, 2014.

[49] L. Duan, W. Yang, K. Bi, S. Chen, Q. Luo, and Q. Liu, "Fast discrimination and counting of filled/unfilled rice spikelets based on bi-modal imaging," *Comput. Electron. Agric.*, vol. 75, no. 1, pp. 196–203, 2011. doi: 10.1016/j.compag.2010.11.004.

[50] F. Cointault, D. Guérin, J. P. Guillemin, and B. Chopinet, "In-field *Triticum aestivum* ear counting using colour-texture image analysis," *N. Z. J. Crop Hortic Sci.*, vol. 36, no. 2, pp. 117–130, 2008. doi: 10.1080/01140670809510227.

[51] F. Cointault and P. Gouton, "Texture or color analysis in agronomic images for wheat ear counting," in *Proc. 2007 3rd Int. IEEE Conf. Signal-Image Technologies and Internet-Based System (SITIS'07)*, pp. 696–701. doi: 10.1109/SITIS.2007.80.

[52] L. Qiongyan, J. Cai, B. Berger, M. Okamoto, and S. J. Miklavcic, "Detecting spikes of wheat plants using neural networks with Laws texture energy," *Plant Methods*, vol. 13, no. 1, p. 83, 2017. doi: 10.1186/s13007-017-0231-1.

[53] D. M. Rubin, "A simple autocorrelation algorithm for determining grain size from digital images of sediment," *J. Sediment. Res.*, vol. 74, no. 1, pp. 160–165, 2004. doi: 10.1306/052203740160.

[54] R. Heilbronner, "Automatic grain boundary detection and grain size analysis using polarization micrographs or orientation images," *J. Struct. Geol.*, vol. 22, no. 7, pp. 969–981, 2000. doi: 10.1016/S0191-8141(00)00014-6.

[55] D. D. Bhosale, "Use of digital image processing for grain counting," *Int. J. Adv. Res. Comput. Sci. Manage. Stud.*, vol. 3, no. 3, pp. 6–9, 2015.

[56] N. D. Miller, N. J. Haase, J. Lee, S. M. Kaeppler, N. Leon, and E. P. Spalding, "A robust, high-throughput method for computing maize ear, cob, and kernel attributes automatically from images," *Plant J.*, vol. 89, no. 1, pp. 169–178, 2017. doi: 10.1111/tpj.13320.

[57] S. Du, L. Liu, X. Liu, and J. Hu, "Response of canopy solar-induced chlorophyll fluorescence to the absorbed photosynthetically active radiation absorbed by chlorophyll," *Remote Sens.*, vol. 9, no. 9, p. 911, 2017. doi: 10.3390/rs9090911.

[58] M. L. Guillén-Climent, P. J. Zarco-Tejada, and F. J. Villalobos, "Estimating radiation interception in heterogeneous orchards using high spatial resolution airborne imagery," *IEEE Geosci. Remote Sens. Lett.*, vol. 11, no. 2, pp. 579–583, 2014. doi: 10.1109/LGRS.2013.2284660.

[59] X. Jin et al., "A review of data assimilation of remote sensing and crop models," *Eur. J. Agron.*, vol. 92, pp. 141–152, Jan. 2018. doi: 10.1016/j.eja.2017.11.002.

[60] G. Zhou, X. Liu, S. Zhao, M. Liu, and L. Wu, "Estimating FAPAR of rice growth period using radiation transfer model coupled with the WOFOST model for analyzing heavy metal stress," *Remote Sens.*, vol. 9, no. 5, p. 424, 2017. doi: 10.3390/rs9050424.

[61] M. Guillen-Climent, P. J. Zarco-Tejada, J. Berni, P. North, and F. Villalobos, "Mapping radiation interception in row-structured orchards using 3D simulation and high-resolution airborne imagery acquired from a UAV," *Precis. Agric.*, vol. 13, no. 4, pp. 473–500, 2012. doi: 10.1007/s11119-012-9263-8.

[62] R. Makanza et al., "High-throughput phenotyping of canopy cover and senescence in maize field trials using aerial digital canopy imaging," *Remote Sens.*, vol. 10, no. 2, p. 330, 2018. doi: 10.3390/rs10020330.

[63] M. S. Lopes and M. P. Reynolds, "Stay-green in spring wheat can be determined by spectral reflectance measurements (normalized difference vegetation index) independently from phenology," *J. Exp. Bot.*, vol. 63, no. 10, pp. 3789–3798, 2012. doi: 10.1093/jxb/ers071.

[64] S. Kipp, B. Mistele, and U. Schmidhalter, "Identification of stay-green and early senescence phenotypes in high-yielding winter wheat, and their relationship to grain yield and grain protein concentration using high-throughput phenotyping techniques," *Funct. Plant Biol.*, vol. 41, no. 3, pp. 227–235, 2014. doi: 10.1071/FP13221.

[65] S. Zahra, "Characterization of a wheat mapping population for growth pattern and studying staygreen wheat canopy using multispectral UAV images," M.S. thesis, Texas A&M Univ., College Station, 2017.

[66] M. A. Hassan et al., "Time-series multispectral indices from unmanned aerial vehicle imagery reveal senescence rate in bread wheat," *Remote Sens.*, vol. 10, no. 6, p. 809, 2018. doi: 10.3390/rs10060809.

[67] U. Schmidhalter et al., "Field-scale validation of a tractor based multispectral crop scanner to determine biomass and nitrogen uptake of winter wheat," in *Proc. 4th European Conf. Precision Agriculture*, Berlin, 2003, pp. 615–619.

[68] M. Babar, M. Reynolds, M. Van Ginkel, A. Klatt, W. Raun, and M. Stone, "Spectral reflectance indices as a potential indirect selection criteria for wheat yield under irrigation," *Crop Sci.*, vol. 46, no. 2, pp. 578–588, 2006. doi: 10.2135/cropsci2005.0059.

[69] M. Babar, M. Reynolds, M. Van Ginkel, A. Klatt, W. Raun, and M. Stone, "Spectral reflectance to estimate genetic variation for in-season biomass, leaf chlorophyll, and canopy temperature in wheat," *Crop Sci.*, vol. 46, no. 3, pp. 1046–1057, 2006. doi: 10.2135/cropsci2005.0211.

[70] T. Duan, S. Chapman, Y. Guo, and B. Zheng, "Dynamic monitoring of NDVI in wheat agronomy and breeding trials using an unmanned aerial vehicle," *Field Crops Res.*, vol. 210, pp. 71–80, Aug. 2017. doi: 10.1016/j.fcr.2017.05.025.

[71] J. A. Berni, P. J. Zarco-Tejada, L. Suárez, and E. Fereres, "Thermal and narrowband multispectral remote sensing for vegetation monitoring from an unmanned aerial vehicle," *IEEE Trans. Geosci. Remote Sens.*, vol. 47, no. 3, pp. 722–738, 2009. doi: 10.1109/TGRS.2008.2010457.

[72] M. A. Uddin, A. Mansour, D. L. Jeune, M. Ayaz, and E.-H. M. Aggoune, "UAV-assisted dynamic clustering of wireless sensor networks for crop health monitoring," *Sensors*, vol. 18, no. 2, p. 555, 2018. doi: 10.3390/s18020555.

[73] J. Li et al., "Field phenotyping: Concepts and examples to quantify dynamic plant traits across scales in the field," in *Terrestrial Ecosystem Research Infrastructures*: Challenges and Opportunities, A. Chabbi and H. W. Loescher, Eds. Boca Raton, FL: CRC, 2017, pp. 77–104.

[74] W. Guo, T. Fukatsu, and S. Ninomiya, "Automated characterization of flowering dynamics in rice using field-acquired time-series RGB images," *Plant Methods*, vol. 11, no. 1, p. 7, 2015. doi: 10.1186/s13007-015-0047-9.

[75] A. E. Fonseca, M. E. Westgate, and R. T. Doyle, "Application of fluorescence microscopy and image analysis for quantifying dynamics of maize pollen shed," *Crop Sci.*, vol. 42, no. 6, pp. 2201–2206, 2002. doi: 10.2135/cropsci2002.2201.

[76] Z. Pan et al., "Mapping crop phenology using NDVI time-series derived from HJ-1 A/B data," *Int. J. Appl. Earth Observ. Geoinform.*, vol. 34, pp. 188–197, Feb. 2015. doi: 10.1016/j.jag.2014.08.011.

[77] L. Zeng et al., "A hybrid approach for detecting corn and soybean phenology with time-series MODIS data," *Remote Sens. Environ.*, vol. 181, pp. 237–250, Aug. 2016. doi: 10.1016/j.rse.2016.03.039.

[78] S. Ren, Q. Qin, and H. Ren, "Contrasting wheat phenological responses to climate change in global scale," *Sci. Total Environ.*, vol. 665, pp. 620–631, May 2019. doi: 10.1016/j.scitotenv.2019.01.394.

[79] P. Jonsson and L. Eklundh, "Seasonality extraction by function fitting to time-series of satellite sensor data," *IEEE Trans. Geosci. Remote Sens.*, vol. 40, no. 8, pp. 1824–1832, 2002. doi: 10.1109/TGRS.2002.802519.

[80] T. Sakamoto, M. Yokozawa, H. Toritani, M. Shibayama, N. Ishitsuka, and H. Ohno, "A crop phenology detection method using time-series MODIS data," *Remote Sens. Environ.*, vol. 96, no. 3–4, pp. 366–374, 2005. doi: 10.1016/j.rse.2005.03.008.

[81] P. S. Beck, C. Atzberger, K. A. Høgda, B. Johansen, and A. K. Skidmore, "Improved monitoring of vegetation dynamics at very high latitudes: A new method using MODIS NDVI," *Remote Sens. Environ.*, vol. 100, no. 3, pp. 321–334, 2006. doi: 10.1016/j.rse.2005.10.021.

[82] B. Duchemin, J. Goubier, and G. Courrier, "Monitoring phenological key stages and cycle duration of temperate deciduous forest ecosystems with NOAA/AVHRR data," *Remote Sens. Environ.*, vol. 67, no. 1, pp. 68–82, 1999. doi: 10.1016/S0034-4257(98)00067-4.

[83] C. Atzberger and P. H. Eilers, "A time series for monitoring vegetation activity and phenology at 10-daily time steps covering large parts of South America," *Int. J. Digit. Earth*, vol. 4, no. 5, pp. 365–386, 2011. doi: 10.1080/17538947.2010.505664.

[84] T. Sakamoto, "Refined shape model fitting methods for detecting various types of phenological information on major US crops," *ISPRS J. Photogramm. Remote Sens.*, vol. 138, pp. 176–192, Apr. 2018. doi: 10.1016/j.isprsjprs.2018.02.011.

[85] A. Verger, I. Filella, F. Baret, and J. Peñuelas, "Vegetation baseline phenology from kilometric global LAI satellite products," *Remote Sens. Environ.*, vol. 178, pp. 1–14, June 2016. doi: 10.1016/j.rse.2016.02.057.

[86] Y. Luo, Z. Zhang, Y. Chen, Z. Li, and F. Tao, "ChinaCropPhen1km: A high-resolution crop phenological dataset for three staple crops in China during 2000–2015 based on leaf area index (LAI) products," *Earth Syst. Sci. Data*, vol. 12, no. 1, pp. 197–214, 2020. doi: 10.5194/essd-12-197-2020.

[87] H. Wang, R. Magagi, K. Goïta, M. Trudel, H. McNairn, and J. Powers, "Crop phenology retrieval via polarimetric SAR decomposition and Random Forest algorithm," *Remote Sens. Environ.*, vol. 231, p. 111,234, Sept. 2019. doi: 10.1016/j.rse.2019.111234.

[88] J. M. Lopez-Sanchez, S. R. Cloude, and J. D. Ballester-Berman, "Rice phenology monitoring by means of SAR polarimetry at X-band," *IEEE Trans. Geosci. Remote Sens.*, vol. 50, no. 7, pp. 2695–2709, 2011. doi: 10.1109/TGRS.2011.2176740.

[89] J. M. Lopez-Sanchez, F. Vicente-Guijalba, J. D. Ballester-Berman, and S. R. Cloude, "Polarimetric response of rice fields at C-band: Analysis and phenology retrieval," *IEEE Trans. Geosci. Remote Sens.*, vol. 52, no. 5, pp. 2977–2993, 2013. doi: 10.1109/TGRS.2013.2268319.

[90] Q. Yang, L. Shi, J. Han, J. Yu, and K. Huang, "A near real-time deep learning approach for detecting rice phenology based on UAV images," *Agric. For. Meteorol.*, vol. 287, p. 107,938, June 2020. doi: 10.1016/j.agrformet.2020.107938.

[91] S. Kipp, B. Mistele, P. Baresel, and U. Schmidhalter, "High-throughput phenotyping early plant vigour of winter wheat," *Eur. J. Agron.*, vol. 52, pp. 271–278, Jan. 2014. doi: 10.1016/j.eja.2013.08.009.

[92] F. Liebisch, N. Kirchgessner, D. Schneider, A. Walter, and A. Hund, "Remote, aerial phenotyping of maize traits with a mobile multi-sensor approach," *Plant Methods*, vol. 11, no. 1, p. 9, 2015. doi: 10.1186/s13007-015-0048-8.

[93] K. Yu, N. Kirchgessner, C. Grieder, A. Walter, and A. Hund, "An image analysis pipeline for automated classification of imaging light conditions and for quantification of wheat canopy cover time series in field phenotyping," *Plant Methods*, vol. 13, no. 1, p. 15, 2017. doi: 10.1186/s13007-017-0168-4.

[94] F. Chianucci, A. Lucibelli, and M. T. Dell'Abate, "Estimation of ground canopy cover in agricultural crops using downward-looking photography," *Biosyst. Eng.*, vol. 169, pp. 209–216, May 2018. doi: 10.1016/j.biosystemseng.2018.02.012.

[95] M. Richardson, D. Karcher, and L. Purcell, "Quantifying turfgrass cover using digital image analysis," *Crop Sci.*, vol. 41, no. 6, pp. 1884–1888, 2001. doi: 10.2135/cropsci2001.1884.

[96] T. J. Trout, L. F. Johnson, and J. Gartung, "Remote sensing of canopy cover in horticultural crops," *HortScience*, vol. 43, no. 2, pp. 333–337, 2008. doi: 10.21273/HORTSCI.43.2.333.

[97] E. Lukina, M. Stone, and W. Raun, "Estimating vegetation coverage in wheat using digital images," *J. Plant Nutr.*, vol. 22, no. 2, pp. 341–350, 1999. doi: 10.1080/01904169909365631.

[98] Y. Fang and R. P. Ramasamy, "Current and prospective methods for plant disease detection," *Biosensors*, vol. 5, no. 3, pp. 537–561, 2015. doi: 10.3390/bios5030537.

[99] S. Nebiker, N. Lack, M. Abächerli, and S. Läderach, "Lightweight multispectral UAV sensors and their capabilities for predicting grain yield and detecting plant diseases," *Int. Arch. Photogramm. Remote Sens. Spat. Inform. Sci.*, vol. 41B1, pp. 963–970, June 2016. doi: 10.5194/isprs-archives-XLI-B1-963-2016.

[100] S. Sankaran, J. M. Maja, S. Buchanon, and R. Ehsani, "Huanglongbing (citrus greening) detection using visible, near infrared and thermal imaging techniques," *Sensors*, vol. 13, no. 2, pp. 2117–2130, 2013. doi: 10.3390/s130202117.

[101] C.-M. Yang, C.-H. Cheng, and R.-K. Chen, "Changes in spectral characteristics of rice canopy infested with brown planthopper and leaffolder," *Crop Sci.*, vol. 47, no. 1, pp. 329–335, 2007. doi: 10.2135/cropsci2006.05.0335.

[102] W.-C. Qin, B.-J. Qiu, X.-Y. Xue, C. Chen, Z.-F. Xu, and Q.-Q. Zhou, "Droplet deposition and control effect of insecticides sprayed with an unmanned aerial vehicle against plant hoppers," *Crop Prot.*, vol. 85, pp. 79–88, July 2016. doi: 10.1016/j.cropro.2016.03.018.

[103] K. Yamamoto, T. Togami, and N. Yamaguchi, "Super-resolution of plant disease images for the acceleration of image-based phenotyping and vigor diagnosis in agriculture," *Sensors*, vol. 17, no. 11, p. 2557, 2017. doi: 10.3390/s17112557.

[104] J. Behmann et al., "Specim IQ: Evaluation of a new, miniaturized handheld hyperspectral camera and its application for plant phenotyping and disease detection," *Sensors*, vol. 18, no. 2, p. 441, 2018. doi: 10.3390/s18020441.

[105] F. Vanegas, D. Bratanov, K. Powell, J. Weiss, and F. Gonzalez, "A novel methodology for improving plant pest surveillance in vineyards and crops using UAV-based hyperspectral and spatial data," *Sensors*, vol. 18, no. 1, p. 260, 2018. doi: 10.3390/s18010260.

[106] T. Rumpf, A.-K. Mahlein, U. Steiner, E.-C. Oerke, H.-W. Dehne, and L. Plümer, "Early detection and classification of plant diseases with support vector machines based on hyperspectral reflectance," *Comput. Electron. Agric.*, vol. 74, no. 1, pp. 91–99, 2010. doi: 10.1016/j.compag.2010.06.009.

[107] J. Bendig et al., "Combining UAV-based plant height from crop surface models, visible, and near infrared vegetation indices for biomass monitoring in barley," *Int. J. Appl. Earth Observ. Geoinform.*, vol. 39, pp. 79–87, July 2015. doi: 10.1016/j.jag.2015.02.012.

[108] D. Anthony, S. Elbaum, A. Lorenz, and C. Detweiler, "On crop height estimation with UAVs," in *Proc. 2014 IEEE/RSJ Int. Conf. Intelligent Robots and Systems (IROS 2014)*, pp. 4805–4812. doi: 10.1109/IROS.2014.6943245.

[109] A. J. Mathews and J. L. Jensen, "Visualizing and quantifying vineyard canopy LAI using an unmanned aerial vehicle (UAV) collected high density structure from motion point cloud," *Remote Sens.*, vol. 5, no. 5, pp. 2164–2183, 2013. doi: 10.3390/rs5052164.

[110] A. Matese, S. F. Di Gennaro, and A. Berton, "Assessment of a canopy height model (CHM) in a vineyard using UAV-based multispectral imaging," *Int. J. Remote Sens.*, vol. 38, no. 8–10, pp. 2150–2160, 2017. doi: 10.1080/01431161.2016.1226002.

[111] G. Barmeier, B. Mistele, and U. Schmidhalter, "Referencing laser and ultrasonic height measurements of barley cultivars by using a herbometre as standard," *Crop Pasture Sci.*, vol. 67, no. 12, pp. 1215–1222, 2017. doi: 10.1071/CP16238.

[112] Q. Guo et al., "Crop 3D: A LiDAR based platform for 3D high-throughput crop phenotyping," *Sci. China Life Sci.*, vol. 61, no. 3, pp. 328–339, 2018. doi: 10.1007/s11427-017-9056-0.

[113] I. Amani, R. Fischer, and M. Reynolds, "Evaluation of canopy temperature as a screening tool for heat tolerance in spring wheat," *J. Agron. Crop Sci.*, vol. 176, no. 2, pp. 119–129, 1996. doi: 10.1111/j.1439-037X.1996.tb00454.x.

[114] L. Winterhalter, B. Mistele, S. Jampatong, and U. Schmidhalter, "High throughput phenotyping of canopy water mass and canopy temperature in well-watered and drought stressed tropical maize hybrids in the vegetative stage," *Eur. J. Agron.*, vol. 35, no. 1, pp. 22–32, 2011. doi: 10.1016/j.eja.2011.03.004.

[115] P. J. Zarco-Tejada, J. A. Berni, L. Suárez, and E. Fereres, "A new era in remote sensing of crops with unmanned robots," *SPIE Newsroom*, pp. 2–4, Jan. 2008. doi: 10.1117/2.1200812.1438.

[116] J. Baluja et al., "Assessment of vineyard water status variability by thermal and multispectral imagery using an unmanned aerial vehicle (UAV)," *Irrig. Sci.*, vol. 30, no. 6, pp. 511–522, 2012. doi: 10.1007/s00271-012-0382-9.

[117] K. Kusnierek and A. Korsaeth, "Challenges in using an analog uncooled microbolometer thermal camera to measure crop temperature," *Int. J. Agric. Biol. Eng.*, vol. 7, no. 4, pp. 60–74, 2014.

[118] R. S. Pinto and M. P. Reynolds, "Common genetic basis for canopy temperature depression under heat and drought stress associated with optimized root distribution in bread wheat," *Theor. Appl. Genet.*, vol. 128, no. 4, pp. 575–585, 2015. doi: 10.1007/s00122-015-2453-9.

[119] C. Panigada et al., "Fluorescence, PRI and canopy temperature for water stress detection in cereal crops," *Int. J. Appl. Earth Observ. Geoinform.*, vol. 30, pp. 167–178, Aug. 2014. doi: 10.1016/j.jag.2014.02.002.

[120] H. Hoffmann, R. Jensen, A. Thomsen, H. Nieto, J. Rasmussen, and T. Friborg, "Crop water stress maps for an entire growing season from visible and thermal UAV imagery," *Biogeosciences*, vol. 13, no. 24, pp. 6545–6563, 2016. doi: 10.5194/bg-13-6545-2016.

[121] P. Rischbeck, P. Cardellach, B. Mistele, and U. Schmidhalter, "Thermal phenotyping of stomatal sensitivity in spring barley," *J. Agron. Crop Sci.*, vol. 203, no. 6, pp. 483–493, 2017. doi: 10.1111/jac.12223.

[122] J. Martínez, G. Egea, J. Agüera, and M. Pérez-Ruiz, "A cost-effective canopy temperature measurement system for precision agriculture: A case study on sugar beet," *Precis. Agric.*, vol. 18, no. 1, pp. 95–110, 2017. doi: 10.1007/s11119-016-9470-9.

[123] A. L. Thompson et al., "Deploying a proximal sensing cart to identify drought adaptive traits in upland cotton for high-throughput phenotyping," *Front. Plant Sci.*, vol. 9, p. 507, Apr. 2018. doi: 10.3389/fpls.2018.00507.

[124] F. Baret et al., "Leaf-rolling in maize crops: From leaf scoring to canopy-level measurements for phenotyping," *J. Exp. Bot.*, vol. 69, no. 10, pp. 2705–2716, 2018. doi: 10.1093/jxb/ery071.

[125] S. Bhugra, A. Anupama, S. Chaudhury, B. Lall, and A. Chugh, "Multi-modal image analysis for plant stress phenotyping," in *Proc. 6th Nat. Conf. Computer Vision, Pattern Recognition, Image Processing, and Graphics (NCVPRIPG 2017)*, Mandi, India, 2018, pp. 269–280. doi: 10.1007/978-981-13-0020-2_24.

[126] X. Sirault, A. Condon, J. Wood, G. Farquhar, and G. Rebetzke, "'Rolled-upness': Phenotyping leaf rolling in cereals using computer vision and functional data analysis approaches," *Plant Methods*, vol. 11, no. 1, p. 52, 2015. doi: 10.1186/s13007-015-0095-1.

[127] X. Mu et al., "Estimating structural parameters of agricultural crops from ground-based multi-angular digital images with a fractional model of sun and shade components," *Agric. For. Meteorol.*, vol. 246, pp. 162–177, Nov. 2017. doi: 10.1016/j.agrformet.2017.06.009.

[128] M. Müller-Linow, F. Pinto-Espinosa, H. Scharr, and U. Rascher, "The leaf angle distribution of natural plant populations: Assessing the canopy with a novel software tool," *Plant Methods*, vol. 11, no. 1, p. 11, 2015. doi: 10.1186/s13007-015-0052-z.

[129] S. Thapa, F. Zhu, H. Walia, H. Yu, and Y. Ge, "A novel LiDAR-based instrument for high-throughput, 3D measurement of morphological traits in maize and sorghum," *Sensors*, vol. 18, no. 4, p. 1187, 2018. doi: 10.3390/s18041187.

[130] B. Biskup, H. Scharr, U. Schurr, and U. Rascher, "A stereo imaging system for measuring structural parameters of plant canopies," *Plant Cell Environ.*, vol. 30, no. 10, pp. 1299–1308, 2007. doi: 10.1111/j.1365-3040.2007.01702.x.

[131] R. Calderón, J. A. Navas-Cortés, C. Lucena, and P. J. Zarco-Tejada, "High-resolution airborne hyperspectral and thermal imagery for early detection of Verticillium wilt of olive using fluorescence, temperature and narrow-band spectral indices," *Remote Sens. Environ.*, vol. 139, pp. 231–245, Dec. 2013. doi: 10.1016/j.rse.2013.07.031.

[132] R. Calderón, J. Navas-Cortés, and P. Zarco-Tejada, "Early detection and quantification of Verticillium wilt in olive using hyperspectral and thermal imagery over large areas," *Remote Sens.*, vol. 7, no. 5, pp. 5584–5610, 2015. doi: 10.3390/rs70505584.

[133] L. Chaerle, S. Lenk, I. Leinonen, H. G. Jones, D. Van Der Straeten, and C. Buschmann, "Multi-sensor plant imaging: Towards the development of a stress-catalogue," *BioTechnol. J.*, vol. 4, no. 8, pp. 1152–1167, 2009. doi: 10.1002/biot.200800242.

[134] T. Liu et al., "Estimates of rice lodging using indices derived from UAV visible and thermal infrared images," *Agric. For. Meteorol.*, vol. 252, pp. 144–154, Apr. 2018. doi: 10.1016/j.agrformet.2018.01.021.

[135] R. T. Ogden, C. E. Miller, K. Takezawa, and S. Ninomiya, "Functional regression in crop lodging assessment with digital images," *J. Agric., Biol., Environ. Stat.*, vol. 7, no. 3, p. 389, 2002. doi: 10.1198/108571102339.

[136] S. C. Chapman et al., "Pheno-copter: A low-altitude, autonomous remote-sensing robotic helicopter for high-throughput field-based phenotyping," *Agronomy*, vol. 4, no. 2, pp. 279–301, 2014. doi: 10.3390/agronomy4020279.

[137] T. Chu, M. J. Starek, M. J. Brewer, T. Masiane, and S. C. Murray, "UAS imaging for automated crop lodging detection: A case study over an experimental maize field," in *Proc. Autonomous Air and Ground Sensing Systems Agricultural Optimization and Phenotyping II*, 2017, vol. 10,218, p. 102180E. doi: 10.1117/12.2262812.

[138] M.-D. Yang, K.-S. Huang, Y.-H. Kuo, H. P. Tsai, and L.-M. Lin, "Spatial and spectral hybrid image classification for rice lodging assessment through UAV imagery," *Remote Sens.*, vol. 9, no. 6, p. 583, 2017. doi: 10.3390/rs9060583.

[139] A. Q. Susko, F. Gilbertson, D. J. Heuschele, K. Smith, and P. Marchetto, "An automatable, field camera track system for phenotyping crop lodging and crop movement," *HardwareX*, vol. 4, p. e00029, Oct. 2018. doi: 10.1016/j.ohx.2018.e00029.

[140] N. Wilke et al., "Quantifying lodging percentage and lodging severity using a UAV-based canopy height model combined with an objective threshold approach," *Remote Sens.*, vol. 11, no. 5, p. 515, 2019. doi: 10.3390/rs11050515.

[141] M.-D. Yang, H.-H. Tseng, Y.-C. Hsu, and H. P. Tsai, "Semantic segmentation using deep learning with vegetation indices for rice lodging identification in multi-date UAV visible images," *Remote Sens.*, vol. 12, no. 4, p. 633, 2020. doi: 10.3390/rs12040633.

[142] S. Chauhan, R. Darvishzadeh, M. Boschetti, and A. Nelson, "Estimation of crop angle of inclination for lodged wheat us-

ing multi-sensor SAR data," *Remote Sens. Environ.*, vol. 236, p. 111,488, Jan. 2020. doi: 10.1016/j.rse.2019.111488.

[143] H. Yang et al., "Wheat lodging monitoring using polarimetric index from RADARSAT-2 data," *Int. J. Appl. Earth Observ. Geoinform.*, vol. 34, pp. 157–166, Feb. 2015. doi: 10.1016/j.jag.2014.08.010.

[144] L. Zhao, J. Yang, P. Li, L. Shi, and L. Zhang, "Characterizing lodging damage in wheat and canola using Radarsat-2 polarimetric SAR data," *Remote Sens. Lett.*, vol. 8, no. 7, pp. 667–675, 2017. doi: 10.1080/2150704X.2017.1312028.

[145] J. Dong, H. Lu, Y. Wang, T. Ye, and W. Yuan, "Estimating winter wheat yield based on a light use efficiency model and wheat variety data," *ISPRS J. Photogramm. Remote Sens.*, vol. 160, pp. 18–32, Feb. 2020. doi: 10.1016/j.isprsjprs.2019.12.005.

[146] C. Bredemeier and U. Schmidhalter, "Laser-induced chlorophyll fluorescence sensing to determine biomass and nitrogen uptake of winter wheat under controlled environment and field conditions," *Precis. Agric.*, pp. 273–280, Jan. 2005.

[147] D. Thoren and U. Schmidhalter, "Nitrogen status and biomass determination of oilseed rape by laser-induced chlorophyll fluorescence," *Eur. J. Agron.*, vol. 30, no. 3, pp. 238–242, 2009. doi: 10.1016/j.eja.2008.12.001.

[148] M. Jansen et al., "Simultaneous phenotyping of leaf growth and chlorophyll fluorescence via GROWSCREEN FLUORO allows detection of stress tolerance in Arabidopsis thaliana and other rosette plants," *Funct. Plant Biol.*, vol. 36, no. 11, pp. 902–914, 2009. doi: 10.1071/FP09095.

[149] D. K. Sharma, S. B. Andersen, C.-O. Ottosen, and E. Rosenqvist, "Phenotyping of wheat cultivars for heat tolerance using chlorophyll a fluorescence," *Funct. Plant Biol.*, vol. 39, no. 11, pp. 936–947, 2012. doi: 10.1071/FP12100.

[150] N. Fahlgren, M. A. Gehan, and I. Baxter, "Lights, camera, action: High-throughput plant phenotyping is ready for a close-up," *Curr. Opin. Plant Biol.*, vol. 24, pp. 93–99, Apr. 2015. doi: 10.1016/j.pbi.2015.02.006.

[151] H. M. Kalaji et al., "Chlorophyll a fluorescence as a tool to monitor physiological status of plants under abiotic stress conditions," *Acta Physiol. Plant.*, vol. 38, no. 4, p. 102, 2016. doi: 10.1007/s11738-016-2113-y.

[152] H. Kalaji et al., "Prompt chlorophyll fluorescence as a tool for crop phenotyping: An example of barley landraces exposed to various abiotic stress factors," *Photosynthetica*, vol. 56, no. 3, pp. 953–961, 2018. doi: 10.1007/s11099-018-0766-z.

[153] R. Zhou et al., "Phenotyping of faba beans (*Vicia faba* L.) under cold and heat stresses using chlorophyll fluorescence," *Euphytica*, vol. 214, no. 4, p. 68, 2018. doi: 10.1007/s10681-018-2154-y.

[154] D. Heckmann, U. Schlüter, and A. P. Weber, "Machine learning techniques for predicting crop photosynthetic capacity from leaf reflectance spectra," *Mol. Plant*, vol. 10, no. 6, pp. 878–890, 2017. doi: 10.1016/j.molp.2017.04.009.

[155] E. Carmo-Silva et al., "Phenotyping of field-grown wheat in the U.K. highlights contribution of light response of photosynthesis and flag leaf longevity to grain yield," *J. Exp. Bot.*, vol. 68, no. 13, pp. 3473–3486, 2017. doi: 10.1093/jxb/erx169.

[156] T. R. Sinclair, L. C. Purcell, and C. H. Sneller, "Crop transformation and the challenge to increase yield potential," *Trends Plant Sci.*, vol. 9, no. 2, pp. 70–75, 2004. doi: 10.1016/j.tplants.2003.12.008.

[157] W. Khan, B. Prithiviraj, and D. L. Smith, "Photosynthetic responses of corn and soybean to foliar application of salicylates," *J. Plant Physiol.*, vol. 160, no. 5, pp. 485–492, 2003. doi: 10.1078/0176-1617-00865.

[158] M. Arfan, H. R. Athar, and M. Ashraf, "Does exogenous application of salicylic acid through the rooting medium modulate growth and photosynthetic capacity in two differently adapted spring wheat cultivars under salt stress?" *J. Plant Physiol.*, vol. 164, no. 6, pp. 685–694, 2007. doi: 10.1016/j.jplph.2006.05.010.

[159] M. Zivcak et al., "Photosynthetic electron transport and specific photoprotective responses in wheat leaves under drought stress," *Photosynth. Res.*, vol. 117, no. 1–3, pp. 529–546, 2013. doi: 10.1007/s11120-013-9885-3.

[160] C. Dong et al., "Photosynthetic characteristics, antioxidant capacity and biomass yield of wheat exposed to intermittent light irradiation with millisecond-scale periods," *J. Plant Physiol.*, vol. 184, pp. 28–36, July 2015. doi: 10.1016/j.jplph.2015.06.012.

[161] B. Mistele and U. Schmidhalter, "Tractor-based quadrilateral spectral reflectance measurements to detect biomass and total aerial nitrogen in winter wheat," *Agron. J.*, vol. 102, no. 2, pp. 499–506, 2010. doi: 10.2134/agronj2009.0282.

[162] R. Ballesteros, J. F. Ortega, D. Hernandez, and M. A. Moreno, "Onion biomass monitoring using UAV-based RGB imaging," *Precis. Agric.*, vol. 19, pp. 840–857, 2018. doi: 10.1007/s11119-018-9560-y.

[163] S. Brocks and G. Bareth, "Estimating barley biomass with crop surface models from oblique RGB imagery," *Remote Sens.*, vol. 10, no. 2, p. 268, 2018. doi: 10.3390/rs10020268.

[164] L. Roth and B. Streit, "Predicting cover crop biomass by lightweight UAS-based RGB and NIR photography: An applied photogrammetric approach," *Precis. Agric.*, vol. 19, no. 1, pp. 93–114, 2018. doi: 10.1007/s11119-017-9501-1.

[165] M. Karpina, M. Jarząbek-Rychard, P. Tymków, and A. Borkowski, "UAV-based automatic tree growth measurement for biomass estimation," *ISPRS- Int. Arch. Photogramm. Remote Sens. Spat. Inform. Sci.*, vol. 41B8, pp. 685–688, June 2016. doi: 10.5194/isprs-archives-XLI-B8-685-2016.

[166] S. V. Bueren and I. Yule, "Multispectral aerial imaging of pasture quality and biomass using unmanned aerial vehicles (UAV)," Accurate and Efficient Use of Nutrients on Farms, Occasional Rep., Massey Univ., Palmerston North, New Zealand, 2013, vol. 26.

[167] W. Li, Z. Niu, H. Chen, D. Li, M. Wu, and W. Zhao, "Remote estimation of canopy height and aboveground biomass of maize using high-resolution stereo images from a low-cost unmanned aerial vehicle system," *Ecol. Indic.*, vol. 67, pp. 637–648, Aug. 2016. doi: 10.1016/j.ecolind.2016.03.036.

[168] X. Jin, G. Yang, Z. Li, X. Xu, J. Wang, and Y. Lan, "Estimation of water productivity in winter wheat using the AquaCrop model with field hyperspectral data," *Precis. Agric.*, vol. 19, no. 1, pp. 1–17, 2018. doi: 10.1007/s11119-016-9469-2.

[169] X. Jin, Z. Li, H. Feng, Z. Ren, and S. Li, "Deep neural network algorithm for estimating maize biomass based on simulated Sentinel 2A vegetation indices and leaf area index," *Crop J.*, vol. 8, no. 1, pp. 87–97, 2020. doi: 10.1016/j.cj.2019.06.005.

[170] X. Jin, Z. Li, H. Feng, Z. Ren, and S. Li, "Estimation of maize yield by assimilating biomass and canopy cover derived from hyperspectral data into the AquaCrop model," *Agric. Water Manage.*, vol. 227, p. 105,846, Jan. 2020. doi: 10.1016/j.agwat.2019.105846.

[171] X. Jin, S. Madec, D. Dutartre, B. de Solan, A. Comar, and F. Baret, "High-throughput measurements of stem characteristics to estimate ear density and above-ground biomass," *Plant Phenomics*, vol. 2019, p. 4,820,305, May 2019. doi: 10.34133/2019/4820305.

[172] P. Ceccato, S. Flasse, S. Tarantola, S. Jacquemoud, and J.-M. Grégoire, "Detecting vegetation leaf water content using reflectance in the optical domain," *Remote Sens. Environ.*, vol. 77, no. 1, pp. 22–33, 2001. doi: 10.1016/S0034-4257(01)00191-2.

[173] M. Gutierrez, M. P. Reynolds, and A. R. Klatt, "Association of water spectral indices with plant and soil water relations in contrasting wheat genotypes," *J. Exp. Bot.*, vol. 61, no. 12, pp. 3291–3303, 2010. doi: 10.1093/jxb/erq156.

[174] R. Colombo et al., "Estimation of leaf and canopy water content in poplar plantations by means of hyperspectral indices and inverse modeling," *Remote Sens. Environ.*, vol. 112, no. 4, pp. 1820–1834, 2008. doi: 10.1016/j.rse.2007.09.005.

[175] A. I. Zygielbaum, A. A. Gitelson, T. J. Arkebauer, and D. C. Rundquist, "Non-destructive detection of water stress and estimation of relative water content in maize," *Geophys. Res. Lett.*, vol. 36, no. 12, p. L12403, 2009. doi: 10.1029/2009GL038906.

[176] X. Jin, X. Xu, X. Song, Z. Li, J. Wang, and W. Guo, "Estimation of leaf water content in winter wheat using grey relational analysis–partial least squares modeling with hyperspectral data," *Agron. J.*, vol. 105, no. 5, pp. 1385–1392, 2013. doi: 10.2134/agronj2013.0088.

[177] A. J. S. Neto, D. de Carvalho Lopes, T. G. F. da Silva, S. O. Ferreira, and J. A. S. Grossi, "Estimation of leaf water content in sunflower under drought conditions by means of spectral reflectance," *Eng. Agric., Environ. Food*, vol. 10, no. 2, pp. 104–108, 2017. doi: 10.1016/j.eaef.2016.11.006.

[178] A. Elsherif, R. Gaulton, and J. Mills, "Estimation of vegetation water content at leaf and canopy level using dual-wavelength commercial terrestrial laser scanners," *Interface Focus*, vol. 8, no. 2, p. 20,170,041, 2018. doi: 10.1098/rsfs.2017.0041.

[179] X. Zhu, T. Wang, A. K. Skidmore, R. Darvishzadeh, K. O. Niemann, and J. Liu, "Canopy leaf water content estimated using terrestrial LiDAR," *Agric. For. Meteorol.*, vol. 232, pp. 152–162, Jan. 2017. doi: 10.1016/j.agrformet.2016.08.016.

[180] C. Zhao, L. Liu, J. Wang, W. Huang, X. Song, and C. Li, "Predicting grain protein content of winter wheat using remote sensing data based on nitrogen status and water stress," *Int. J. Appl. Earth Observ. Geoinform.*, vol. 7, no. 1, pp. 1–9, 2005. doi: 10.1016/j.jag.2004.10.002.

[181] J.-h. Wang, W.-j. Huang, C.-j. Zhao, M.-h. Yang, and Z.-j. Wang, "The inversion of leaf biochemical components and grain quality indicators of winter wheat with spectral reflectance," *J. Remote Sens.*, vol. 7, no. 4, pp. 277–284, 2003.

[182] H. Wenjiang, W. Jihua, W. Zhijie, Z. Jiang, L. Liangyun, and W. Jindi, "Inversion of foliar biochemical parameters at various physiological stages and grain quality indicators of winter wheat with canopy reflectance," *Int. J. Remote Sens.*, vol. 25, no. 12, pp. 2409–2419, 2004. doi: 10.1080/01431160310001618095.

[183] W. R. Raun et al., "In-season prediction of potential grain yield in winter wheat using canopy reflectance," *Agron. J.*, vol. 93, no. 1, pp. 131–138, 2001. doi: 10.2134/agronj2001.931131x.

[184] S. Mahesh, A. Manickavasagan, D. Jayas, J. Paliwal, and N. White, "Feasibility of near-infrared hyperspectral imaging to differentiate Canadian wheat classes," *Biosyst. Eng.*, vol. 101, no. 1, pp. 50–57, 2008. doi: 10.1016/j.biosystemseng.2008.05.017.

[185] A. C. Mutlu et al., "Prediction of wheat quality parameters using near-infrared spectroscopy and artificial neural networks," *Eur. Food Res. Technol.*, vol. 233, no. 2, pp. 267–274, 2011. doi: 10.1007/s00217-011-1515-8.

[186] H. Shi and P. Yu, "Comparison of grating-based near-infrared (NIR) and Fourier transform mid-infrared (ATR-FT/MIR) spectroscopy based on spectral preprocessing and wavelength selection for the determination of crude protein and moisture content in wheat," *Food Control*, vol. 82, pp. 57–65, Dec. 2017. doi: 10.1016/j.foodcont.2017.06.015.

[187] Z. Li et al., "Estimating wheat yield and quality by coupling the DSSAT-CERES model and proximal remote sensing," *Eur. J. Agron.*, vol. 71, pp. 53–62, Nov. 2015. doi: 10.1016/j.eja.2015.08.006.

[188] X. Song, G. Yang, C. Yang, J. Wang, and B. Cui, "Spatial variability analysis of within-field winter wheat nitrogen and grain quality using canopy fluorescence sensor measurements," *Remote Sens.*, vol. 9, no. 3, p. 237, 2017. doi: 10.3390/rs9030237.

[189] X. Mo, S. Liu, Z. Lin, Y. Xu, Y. Xiang, and T. McVicar, "Prediction of crop yield, water consumption and water use efficiency with a SVAT-crop growth model using remotely sensed data on the North China Plain," *Ecol. Model.*, vol. 183, nos. 2–3, pp. 301–322, 2005. doi: 10.1016/j.ecolmodel.2004.07.032.

[190] C. Tucker and P. Sellers, "Satellite remote sensing of primary production," *Int. J. Remote Sens.*, vol. 7, no. 11, pp. 1395–1416, 1986. doi: 10.1080/01431168608948944.

[191] S. Er-Raki, A. Chehbouni, N. Guemouria, B. Duchemin, J. Ezzahar, and R. Hadria, "Combining FAO-56 model and ground-based remote sensing to estimate water consumptions of wheat crops in a semi-arid region," *Agric. Water Manage.*, vol. 87, no. 1, pp. 41–54, 2007. doi: 10.1016/j.agwat.2006.02.004.

[192] H. Li, L. Zheng, Y. Lei, C. Li, Z. Liu, and S. Zhang, "Estimation of water consumption and crop water productivity of winter wheat in North China Plain using remote sensing technology," *Agric. Water Manage.*, vol. 95, no. 11, pp. 1271–1278, 2008. doi: 10.1016/j.agwat.2008.05.003.

[193] S. Er-Raki, A. Chehbouni, and B. Duchemin, "Combining satellite remote sensing data with the FAO-56 dual approach for water use mapping in irrigated wheat fields of a semi-arid region," *Remote Sens.*, vol. 2, no. 1, pp. 375–387, 2010. doi: 10.3390/rs2010375.

[194] X. Wu, J. Zhou, H. Wang, Y. Li, and B. Zhong, "Evaluation of irrigation water use efficiency using remote sensing in the middle reach of the Heihe river, in the semi-arid Northwestern China," *Hydrol. Process.*, vol. 29, no. 9, pp. 2243–2257, 2015. doi: 10.1002/hyp.10365.

[195] B. Duchemin et al., "Impact of sowing date on yield and water use efficiency of wheat analyzed through spatial modeling and FORMOSAT-2 images," *Remote Sens.*, vol. 7, no. 5, pp. 5951–5979, 2015. doi: 10.3390/rs70505951.

[196] I. Campos, C. M. Neale, T. J. Arkebauer, A. E. Suyker, and I. Z. Gonçalves, "Water productivity and crop yield: A simplified remote sensing driven operational approach," *Agric. For. Meteorol.*, vol. 249, pp. 501–511, Feb. 2018. doi: 10.1016/j.agrformet.2017.07.018.

[197] F. Hosoi and K. Omasa, "Estimating vertical plant area density profile and growth parameters of a wheat canopy at different growth stages using three-dimensional portable LiDAR imaging," *ISPRS J. Photogramm. Remote Sens.*, vol. 64, no. 2, pp. 151–158, 2009. doi: 10.1016/j.isprsjprs.2008.09.003.

[198] F. Hosoi, K. Nakabayashi, and K. Omasa, "3-D modeling of tomato canopies using a high-resolution portable scanning LiDAR for extracting structural information," *Sensors*, vol. 11, no. 2, pp. 2166–2174, 2011. doi: 10.3390/s110202166.

[199] S. Liu et al., "Estimating wheat green area index from ground-based LiDAR measurement using a 3D canopy structure model," *Agric. For. Meteorol.*, vol. 247, pp. 12–20, Dec. 2017. doi: 10.1016/j.agrformet.2017.07.007.

[200] J. A. Jimenez-Berni et al., "High throughput determination of plant height, ground cover, and above-ground biomass in wheat with LiDAR," *Front. Plant Sci.*, vol. 9, pp. 237, Feb. 2018. doi: 10.3389/fpls.2018.00237.

[201] F. Hui et al., "Image-based dynamic quantification and high-accuracy 3D evaluation of canopy structure of plant populations," *Ann. Bot.*, vol. 121, no. 5, pp. 1079–1088, 2018. doi: 10.1093/aob/mcy016.

[202] R. Reis, "Evaluation of phenotyping methods for maize," M.S. thesis, Univ. of Illinois at Urbana-Champaign, Champaign, 2014.

[203] S. Paulus, J. Behmann, A.-K. Mahlein, L. Plümer, and H. Kuhlmann, "Low-cost 3D systems: Suitable tools for plant phenotyping," *Sensors*, vol. 14, no. 2, pp. 3001–3018, 2014. doi: 10.3390/s140203001.

[204] S. Paulus, J. Dupuis, S. Riedel, and H. Kuhlmann, "Automated analysis of barley organs using 3D laser scanning: An approach for high throughput phenotyping," *Sensors*, vol. 14, no. 7, pp. 12,670–12,686, 2014. doi: 10.3390/s140712670.

[205] J. M. Pena, J. Torres-Sánchez, A. I. de Castro, M. Kelly, and F. López-Granados, "Weed mapping in early-season maize fields using object-based analysis of unmanned aerial vehicle (UAV) images," *PloS One*, vol. 8, no. 10, p. e77151, 2013. doi: 10.1371/journal.pone.0077151.

[206] J. M. Peña, J. Torres-Sánchez, A. Serrano-Pérez, A. I. de Castro, and F. López-Granados, "Quantifying efficacy and limits of unmanned aerial vehicle (UAV) technology for weed seedling detection as affected by sensor resolution," *Sensors*, vol. 15, no. 3, pp. 5609–5626, 2015. doi: 10.3390/s150305609.

[207] F. López-Granados, "Weed detection for site-specific weed management: Mapping and real-time approaches," *Weed Res.*, vol. 51, no. 1, pp. 1–11, 2011. 10.1111/j.1365-3180.2010.00829.x.

[208] F. López-Granados, J. Torres-Sánchez, A. Serrano-Pérez, A. I. de Castro, F.-J. Mesas-Carrascosa, and J.-M. Peña, "Early season weed mapping in sunflower using UAV technology: Variability of herbicide treatment maps against weed thresholds," *Precis. Agr.*, vol. 17, no. 2, pp. 183–199, 2016. doi: 10.1007/s11119-015-9415-8.

[209] M. Pérez-Ortiz, J. M. Peña, P. A. Gutiérrez, J. Torres-Sánchez, C. Hervás-Martínez, and F. López-Granados, "Selecting patterns and features for between-and within-crop-row weed mapping using UAV-imagery," *Expert Syst. Appl.*, vol. 47, pp. 85–94, 2016. doi: 10.1016/j.eswa.2015.10.043.

[210] M. Louargant, S. Villette, G. Jones, N. Vigneau, J. Paoli, and C. Gée, "Weed detection by UAV: Simulation of the impact of spectral mixing in multispectral images," *Precis. Agr.*, vol. 18, no. 6, pp. 932–951, 2017. doi: 10.1007/s11119-017-9528-3.

[211] A. Tewes and J. Schellberg, "Towards remote estimation of radiation use efficiency in maize using UAV-based low-cost camera imagery," *Agronomy*, vol. 8, no. 2, p. 16, 2018. doi: 10.3390/agronomy8020016.

[212] B. Hao et al., "Radiation-use efficiency, biomass production, and grain yield in two maize hybrids differing in drought tolerance," *J. Agron. Crop Sci.*, vol. 202, no. 4, pp. 269–280, 2016. doi: 10.1111/jac.12154.

[213] S. Steinmetz, M. Guerif, R. Delecolle, and F. Baret, "Spectral estimates of the absorbed photosynthetically active radiation and light-use efficiency of a winter wheat crop subjected to nitrogen and water deficiencies," *Remote Sens.*, vol. 11, no. 10, pp. 1797–1808, 1990. doi: 10.1080/01431169008955130.

[214] Y. Nouvellon et al., "Time course of radiation use efficiency in a shortgrass ecosystem: Consequences for remotely sensed estimation of primary production," *Remote Sens. Environ.*, vol. 71, no. 1, pp. 43–55, 2000. doi: 10.1016/S0034-4257(99)00063-2.

[215] Y. Inoue and J. Peñuelas, "Relationship between light use efficiency and photochemical reflectance index in soybean leaves as affected by soil water content," *Int. J. Remote Sens.*, vol. 27, no. 22, pp. 5109–5114, 2006. doi: 10.1080/01431160500373039.

[216] A. A. Gitelson, Y. Peng, T. J. Arkebauer, and A. E. Suyker, "Productivity, absorbed photosynthetically active radiation, and light use efficiency in crops: Implications for remote sensing of crop primary production," *J. Plant Physiol.*, vol. 177, pp. 100–109, Apr. 2015. doi: 10.1016/j.jplph.2014.12.015.

[217] L. Cabrera-Bosquet, C. Fournier, N. Brichet, C. Welcker, B. Suard, and F. Tardieu, "High-throughput estimation of incident light, light interception and radiation-use efficiency of thousands of plants in a phenotyping platform," *New Phytol.*, vol. 212, no. 1, pp. 269–281, 2016. doi: 10.1111/nph.14027.

[218] P. Wagle, Y. Zhang, C. Jin, and X. Xiao, "Comparison of solar-induced chlorophyll fluorescence, light-use efficiency, and process-based GPP models in maize," *Ecol. Appl.*, vol. 26, no. 4, pp. 1211–1222, 2016. doi: 10.1890/15-1434.

[219] S. C. Kefauver et al., "Comparative UAV and field phenotyping to assess yield and nitrogen use efficiency in hybrid and conventional barley," *Front. Plant Sci.*, vol. 8, p. 1733, Oct. 2017. doi: 10.3389/fpls.2017.01733.

[220] R. Roten et al., "Urine patch detection using LiDAR technology to improve nitrogen use efficiency in grazed pastures," *Comput. Electron. Agr.*, vol. 135, pp. 128–133, Apr. 2017. doi: 10.1016/j.compag.2017.02.006.

[221] F. Li et al., "In-season optical sensing improves nitrogen-use efficiency for winter wheat," *Soil Sci. Soc. Amer. J.*, vol. 73, no. 5, pp. 1566–1574, 2009. doi: 10.2136/sssaj2008.0150.

[222] K. Pavuluri, B. Chim, C. Griffey, M. Reiter, M. Balota, and W. Thomason, "Canopy spectral reflectance can predict grain nitrogen use efficiency in soft red winter wheat," *Precis. Agr.*, vol. 16, no. 4, pp. 405–424, 2015. doi: 10.1007/s11119-014-9385-2.

[223] K. Frels, M. Guttieri, B. Joyce, B. Leavitt, and P. S. Baenziger, "Evaluating canopy spectral reflectance vegetation indices to estimate nitrogen use traits in hard winter wheat," *Field Crops Res.*, vol. 217, pp. 82–92, Mar. 2018. doi: 10.1016/j.fcr.2017.12.004.

[224] W. R. Raun et al., "Improving nitrogen use efficiency in cereal grain production with optical sensing and variable rate application," *Agron. J.*, vol. 94, no. 4, pp. 815–820, 2002. doi: 10.2134/agronj2002.0815.

[225] P. Chen, D. Haboudane, N. Tremblay, J. Wang, P. Vigneault, and B. Li, "New spectral indicator assessing the efficiency of crop nitrogen treatment in corn and wheat," *Remote Sens. Environ.*, vol. 114, no. 9, pp. 1987–1997, 2010. doi: 10.1016/j.rse.2010.04.006.

[226] G. N. Nguyen and S. Kant, "Improving nitrogen use efficiency in plants: Effective phenotyping in conjunction with agronomic and genetic approaches," *Funct. Plant Biol.*, vol. 45, no. 6, pp. 606–619, 2018. doi: 10.1071/FP17266.

[227] C. Ravier, M. Quemada, and M.-H. Jeuffroy, "Use of a chlorophyll meter to assess nitrogen nutrition index during the growth cycle in winter wheat," *Field Crops Res.*, vol. 214, pp. 73–82, Dec. 2017. doi: 10.1016/j.fcr.2017.08.023.

[228] B. Zhao et al., "Exploring new spectral bands and vegetation indices for estimating nitrogen nutrition index of summer maize," *Eur. J. Agron.*, vol. 93, pp. 113–125, Feb. 2018. doi: 10.1016/j.eja.2017.12.006.

[229] B. Mistele and U. Schmidhalter, "Estimating the nitrogen nutrition index using spectral canopy reflectance measurements," *Eur. J. Agron.*, vol. 29, no. 4, pp. 184–190, 2008. doi: 10.1016/j.eja.2008.05.007.

[230] K. Erdle, B. Mistele, and U. Schmidhalter, "Comparison of active and passive spectral sensors in discriminating biomass parameters and nitrogen status in wheat cultivars," *Field Crops Res.*, vol. 124, no. 1, pp. 74–84, 2011. doi: 10.1016/j.fcr.2011.06.007.

[231] X. Jin et al., "Estimation of wheat nitrogen status under drip irrigation with canopy spectral indices," *J. Agr. Sci.*, vol. 153, no. 7, pp. 1281–1291, 2015. doi: 10.1017/S0021859614001014.

[232] T. Xia, Y. Miao, D. Wu, H. Shao, R. Khosla, and G. Mi, "Active optical sensing of spring maize for in-season diagnosis of nitrogen status based on nitrogen nutrition index," *Remote Sens.*, vol. 8, no. 7, p. 605, 2016. doi: 10.3390/rs8070605.

[233] H. Yang, J. Yang, F. Li, and N. Liu, "Replacing the nitrogen nutrition index by SPAD values and analysis of effect factors for estimating rice nitrogen status," *Agron. J.*, vol. 110, no. 2, pp. 545–554, 2018. doi: 10.2134/agronj2017.09.0532.

[234] T. Sakamoto, "Incorporating environmental variables into a MODIS-based crop yield estimation method for United States corn and soybeans through the use of a random forest regression algorithm," *ISPRS J. Photogram. Remote Sens.*, vol. 160, pp. 208–228, Feb. 2020. doi: 10.1016/j.isprsjprs.2019.12.012.

[235] M. Maimaitijiang, V. Sagan, P. Sidike, S. Hartling, F. Esposito, and F. B. Fritschi, "Soybean yield prediction from UAV using multimodal data fusion and deep learning," *Remote Sens. Environ.*, vol. 237, p. 111,599, Feb. 2020. doi: 10.1016/j.rse.2019.111599.

[236] R. A. Schwalbert, T. Amado, G. Corassa, L. P. Pott, P. V. Prasad, and I. A. Ciampitti, "Satellite-based soybean yield forecast: Integrating machine learning and weather data for improving crop yield prediction in southern Brazil," *Agric. For. Meteorol.*, vol. 284, p. 107,886, Apr. 2020. doi: 10.1016/j.agrformet.2019.107886.

[237] M. Zhang, J. Zhou, K. A. Sudduth, and N. R. Kitchen, "Estimation of maize yield and effects of variable-rate nitrogen application using UAV-based RGB imagery," *Biosyst. Eng.*, vol. 189, pp. 24–35, Jan. 2020. doi: 10.1016/j.biosystemseng.2019.11.001.

[238] Q. Yang, L. Shi, J. Han, Y. Zha, and P. Zhu, "Deep convolutional neural networks for rice grain yield estimation at the ripening stage using UAV-based remotely sensed images," *Field Crops Res.*, vol. 235, pp. 142–153, Apr. 2019. doi: 10.1016/j.fcr.2019.02.022.

[239] D. B. Lobell, S. Di Tommaso, C. You, I. Yacoubou Djima, M. Burke, and T. Kilic, "Sight for Sorghums: Comparisons of satellite-and ground-based sorghum yield estimates in Mali," *Remote Sensing*, vol. 12, no. 1, p. 100, 2020. doi: 10.3390/rs12010100.

[240] Z. Li et al., "A hierarchical interannual wheat yield and grain protein prediction model using spectral vegetative indices and meteorological data," *Field Crops Res.*, vol. 248, p. 107,711, Mar. 2020. doi: 10.1016/j.fcr.2019.107711.

[241] P. Filippi et al., "An approach to forecast grain crop yield using multi-layered, multi-farm data sets and machine learning," *Precis. Agr.*, vol. 20, no. 5, pp. 1015–1029, 2019. doi: 10.1007/s11119-018-09628-4.

[242] J. Wang et al., "Field-scale rice yield estimation using Sentinel-1A Synthetic Aperture Radar (SAR) data in coastal saline region of Jiangsu Province, China," *Remote Sens.*, vol. 11, no. 19, p. 2274, 2019. doi: 10.3390/rs11192274.

[243] X. Jin et al., "Winter wheat yield estimation based on multi-source medium resolution optical and radar imaging data and the AquaCrop model using the particle swarm optimization algorithm," *ISPRS J. Photogram. Remote Sens.*, vol. 126, pp. 24–37, Apr. 2017. doi: 10.1016/j.isprsjprs.2017.02.001.

[244] X. Jin, L. Kumar, Z. Li, X. Xu, G. Yang, and J. Wang, "Estimation of winter wheat biomass and yield by combining the Aquacrop model and field hyperspectral data," *Remote Sens.*, vol. 8, no. 12, p. 972, 2016. doi: 10.3390/rs8120972.

[245] Z. Li et al., "Assimilation of two variables derived from hyperspectral data into the DSSAT-CERES model for grain yield and quality estimation," *Remote Sens.*, vol. 7, no. 9, pp. 12,400–12,418, 2015. doi: 10.3390/rs70912400.

[246] M. Cosgrove-Davies and L. Goodfriend, "A system for measurement of photosynthesis in the aerial portion of a plant."

[247] L. Li, Q. Zhang, and D. Huang, "A review of imaging techniques for plant phenotyping," *Sensors*, vol. 14, no. 11, pp. 20,078–20,111, 2014. doi: 10.3390/s141120078.

[248] L. Chaerle and D. Van Der Straeten, "Seeing is believing: Imaging techniques to monitor plant health," *Biochimica et Biophysica Acta (BBA)-Gene Structure Expression*, vol. 1519, no. 3, pp. 153–166, 2001. doi: 10.1016/S0167-4781(01)00238-X.

[249] C. Buschmann and H. K. Lichtenthaler, "Principles and characteristics of multi-colour fluorescence imaging of plants," *J. Plant Physiol.*, vol. 152, nos. 2–3, pp. 297–314, 1998. doi: 10.1016/S0176-1617(98)80144-2.

[250] C. Buschmann, G. Langsdorf, and H. Lichtenthaler, "Imaging of the blue, green, and red fluorescence emission of plants: An

overview," *Photosynthetica*, vol. 38, no. 4, pp. 483–491, 2000. doi: 10.1023/A:1012440903014.

[251] R. Steele, *Understanding and Measuring the Shelf-Life of Food*. Woodhead Publishing, 2004.

[252] P. Rischbeck, S. Elsayed, B. Mistele, G. Barmeier, K. Heil, and U. Schmidhalter, "Data fusion of spectral, thermal and canopy height parameters for improved yield prediction of drought stressed spring barley," *Eur. J. Agron.*, vol. 78, pp. 44–59, Aug. 2016. doi: 10.1016/j.eja.2016.04.013.

[253] D. G. Green, "Visual resolution when light enters the eye through different parts of the pupil," *J. Physiol.*, vol. 190, no. 3, p. 583, 1967. doi: 10.1113/jphysiol.1967.sp008229.

[254] Y. Kong et al., "Novel and automatic rice thickness extraction based on photogrammetry using rice edge features," *Sensors*, vol. 19, no. 24, p. 5561, 2019. doi: 10.3390/s19245561.

[255] L. Wallace, A. Lucieer, C. Watson, and D. Turner, "Development of a UAV-LiDAR system with application to forest inventory," *Remote Sens.*, vol. 4, no. 6, pp. 1519–1543, 2012. doi: 10.3390/rs4061519.

[256] M. Brown, A. Majumder, and R. Yang, "Camera-based calibration techniques for seamless multiprojector displays," *IEEE Trans. Vis. Comput. Graphics*, vol. 11, no. 2, pp. 193–206, 2005. doi: 10.1109/TVCG.2005.27.

[257] P. Jackman, D.-W. Sun, and G. ElMasry, "Robust colour calibration of an imaging system using a colour space transform and advanced regression modelling," *Meat Sci.*, vol. 91, no. 4, pp. 402–407, 2012. doi: 10.1016/j.meatsci.2012.02.014.

[258] H. Zheng et al., "Evaluation of RGB, color-infrared and multispectral images acquired from unmanned aerial systems for the estimation of nitrogen accumulation in rice," *Remote Sens.*, vol. 10, no. 6, p. 824, 2018. doi: 10.3390/rs10060824.

[259] M. Tattaris, M. P. Reynolds, and S. C. Chapman, "A direct comparison of remote sensing approaches for high-throughput phenotyping in plant breeding," *Front. Plant Sci.*, vol. 7, p. 1131, Aug. 2016. doi: 10.3389/fpls.2016.01131.

[260] A. Chapman and M. Mesbahi, "UAV swarms: Models and effective interfaces," in *Handbook of Unmanned Aerial Vehicles*, K. Valavanis and G. Vachtsevanos, Eds. Dordrecht, The Netherlands: Springer-Verlag, 2015, pp. 1987–2019.

[261] J. Rasmussen, G. Ntakos, J. Nielsen, J. Svensgaard, R. N. Poulsen, and S. Christensen, "Are vegetation indices derived from consumer-grade cameras mounted on UAVs sufficiently reliable for assessing experimental plots?" *Eur J. Agron.*, vol. 74, pp. 75–92, Mar. 2016. doi: 10.1016/j.eja.2015.11.026.

[262] H. Wang, "Crop assessment and monitoring using optical sensors," Ph. D. dissertation, Kansas State Univ., Manhattan, 2017.

[263] E. D. Kyzivat et al., "A high-resolution airborne color-infrared camera water mask for the NASA ABoVE campaign," *Remote Sens.*, vol. 11, no. 18, p. 2163, 2019. doi: 10.3390/rs11182163.

[264] H. Aasen, E. Honkavaara, A. Lucieer, and P. Zarco-Tejada, "Quantitative remote sensing at ultra-high resolution with UAV spectroscopy: A review of sensor technology, measurement procedures, and data correction workflows," *Remote Sens.*, vol. 10, no. 7, p. 1091, 2018. doi: 10.3390/rs10071091.

[265] P. Zarco-Tejada et al., "Previsual symptoms of Xylella fastidiosa infection revealed in spectral plant-trait alterations," *Nature Plants*, vol. 4, no. 7, pp. 432–439, 2018. doi: 10.1038/s41477-018-0189-7.

[266] P. J. Zarco-Tejada, V. González-Dugo, and J. A. Berni, "Fluorescence, temperature and narrow-band indices acquired from a UAV platform for water stress detection using a micro-hyperspectral imager and a thermal camera," *Remote Sens. Environ.*, vol. 117, pp. 322–337, Feb. 2012. doi: 10.1016/j.rse.2011.10.007.

[267] V. Gonzalez-Dugo, P. Hernandez, I. Solis, and P. Zarco-Tejada, "Using high-resolution hyperspectral and thermal airborne imagery to assess physiological condition in the context of wheat phenotyping," *Remote Sens.*, vol. 7, no. 10, pp. 13,586–13,605, 2015. doi: 10.3390/rs71013586.

[268] H. G. Jones, R. Serraj, B. R. Loveys, L. Xiong, A. Wheaton, and A. H. Price, "Thermal infrared imaging of crop canopies for the remote diagnosis and quantification of plant responses to water stress in the field," *Funct. Plant Biol.*, vol. 36, no. 11, pp. 978–989, 2009. doi: 10.1071/FP09123.

[269] G. Gaussorgues, *La thermographie infrarouge: Principes-technologie-applications*. Paris: Technique et Documentation, 1984.

[270] V. Sagan et al., "UAV-based high resolution thermal imaging for vegetation monitoring, and plant phenotyping using ICI 8640 P, FLIR VUE pro r 640, and thermoMap cameras," *Remote Sens.*, vol. 11, no. 3, p. 330, 2019. doi: 10.3390/rs11030330.

[271] J. Kelly et al., "Challenges and best practices for deriving temperature data from an uncalibrated UAV thermal infrared camera," *Remote Sens.*, vol. 11, no. 5, p. 567, 2019. doi: 10.3390/rs11050567.

[272] B. Bergkamp, S. Impa, A. Asebedo, A. Fritz, and S. K. Jagadish, "Prominent winter wheat varieties response to post-flowering heat stress under controlled chambers and field based heat tents," *Field Crops Res.*, vol. 222, pp. 143–152, June 2018. doi: 10.1016/j.fcr.2018.03.009.

[273] K. Banerjee, P. Krishnan, and N. Mridha, "Application of thermal imaging of wheat crop canopy to estimate leaf area index under different moisture stress conditions," *Biosyst. Eng.*, vol. 166, pp. 13–27, Feb. 2018. doi: 10.1016/j.biosystemseng.2017.10.012.

[274] G. Barmeier, K. Hofer, and U. Schmidhalter, "Mid-season prediction of grain yield and protein content of spring barley cultivars using high-throughput spectral sensing," *Eur. J. Agron.*, vol. 90, pp. 108–116, Oct. 2017. doi: 10.1016/j.eja.2017.07.005.

[275] A. D. Richardson et al., "Tracking vegetation phenology across diverse North American biomes using PhenoCam imagery," *Sci. Data*, vol. 5, no. 1, p. 180,028, 2018. doi: 10.1038/s41597-019-0229-9.

[276] A. Comar, P. Burger, B. de Solan, F. Baret, F. Daumard, and J.-F. Hanocq, "A semi-automatic system for high throughput phenotyping wheat cultivars in-field conditions: Description and first results," *Funct. Plant Biol.*, vol. 39, no. 11, pp. 914–924, 2012. doi: 10.1071/FP12065.

[277] J. Underwood, A. Wendel, B. Schofield, L. McMurray, and R. Kimber, "Efficient in-field plant phenomics for row-crops with an autonomous ground vehicle," *J. Field Robot.*, vol. 34, no. 6, pp. 1061–1083, 2017. doi: 10.1002/rob.21728.

[278] G. Barmeier and U. Schmidhalter, "High-throughput field phenotyping of leaves, leaf sheaths, culms and ears of spring barley cultivars at anthesis and dough ripeness," *Front. Plant Sci.*, vol. 8, p. 1920, 2017. doi: 10.3389/fpls.2017.01920.

[279] N. Virlet, K. Sabermanesh, P. Sadeghi-Tehran, and M. J. Hawkesford, “Field Scanalyzer: An automated robotic field phenotyping platform for detailed crop monitoring,” *Funct. Plant Biol.*, vol. 44, no. 1, pp. 143–153, 2017. doi: 10.1071/FP16163.

[280] M. Friedli, N. Kirchgessner, C. Grieder, F. Liebisch, M. Mannale, and A. Walter, “Terrestrial 3D laser scanning to track the increase in canopy height of both monocot and dicot crop species under field conditions,” *Plant Methods, J. Art.*, vol. 12, no. 1, p. 9, Jan. 29, 2016. doi: 10.1186/s13007-016-0109-7.

[281] C. Zhang and J. M. Kovacs, “The application of small unmanned aerial systems for precision agriculture: A review,” *Precis. Agr.*, vol. 13, no. 6, pp. 693–712, 2012. doi: 10.1007/s11119-012-9274-5.

[282] F. H. Holman, A. B. Riche, M. Castle, M. J. Wooster, and M. J. Hawkesford, “Radiometric calibration of ‘commercial off the shelf’ cameras for UAV-based high-resolution temporal crop phenotyping of reflectance and NDVI,” *Remote Sens.*, vol. 11, no. 14, p. 1657, 2019. doi: 10.3390/rs11141657.

[283] F. Holman, A. Riche, A. Michalski, M. Castle, M. Wooster, and M. Hawkesford, “High throughput field phenotyping of wheat plant height and growth rate in field plot trials using UAV based remote sensing,” *Remote Sens.*, vol. 8, no. 12, p. 1031, 2016. doi: 10.3390/rs8121031.

[284] X. Jin, J. Ma, Z. Wen, and K. Song, “Estimation of maize residue cover using Landsat-8 OLI image spectral information and textural features,” *Remote Sens.*, vol. 7, no. 11, pp. 14,559–14,575, 2015. doi: 10.3390/rs71114559.

[285] W. Koppe et al., “Rice monitoring with multi-temporal and dual-polarimetric TerraSAR-X data,” *Int. J. Appl. Earth Observ. Geoinform.*, vol. 21, pp. 568–576, Apr. 2013. doi: 10.1016/j.jag.2012.07.016.

[286] I. M. Johnstone and M. Raimondo, “Periodic boxcar deconvolution and diophantine approximation,” *Ann. Statist.*, vol. 32, no. 5, pp. 1781–1804, 2004. doi: 10.1214/009053604000000391.

[287] J.-S. Lee and E. Pottier, *Polarimetric Radar Imaging: From Basics to Applications*. Boca Raton, FL: CRC, 2017.

[288] Y. Sheng and D. E. Alsdorf, “Automated georeferencing and orthorectification of Amazon basin-wide SAR mosaics using SRTM DEM data,” *IEEE Trans. Geosci. Remote Sens.*, vol. 43, no. 8, pp. 1929–1940, 2005. doi: 10.1109/TGRS.2005.852160.

[289] M. Brown, K. De Beurs, and M. Marshall, “Global phenological response to climate change in crop areas using satellite remote sensing of vegetation, humidity and temperature over 26 years,” *Remote Sens. Environ.*, vol. 126, pp. 174–183, Nov. 2012. doi: 10.1016/j.rse.2012.08.009.

[290] I. Becker-Reshef et al., “Monitoring global croplands with coarse resolution earth observations: The Global Agriculture Monitoring (GLAM) project,” *Remote Sens.*, vol. 2, no. 6, pp. 1589–1609, 2010. doi: 10.3390/rs2061589.

[291] X.-P. Song et al., “National-scale soybean mapping and area estimation in the United States using medium resolution satellite imagery and field survey,” *Remote Sens. Environ.*, vol. 190, pp. 383–395, Mar. 2017. doi: 10.1016/j.rse.2017.01.008.

[292] C. M. Biradar et al., “A global map of rainfed cropland areas (GMRCA) at the end of last millennium using remote sensing,” *Int. J. Appl. Earth Observ. Geoinform.*, vol. 11, no. 2, pp. 114–129, 2009. doi: 10.1016/j.jag.2008.11.002.

[293] N. Yang et al., “Large-scale crop mapping based on machine learning and parallel computation with grids,” *Remote Sens.*, vol. 11, no. 12, p. 1500, 2019. doi: 10.3390/rs11121500.

[294] B. D. Wardlow and S. L. Egbert, “Large-area crop mapping using time-series MODIS 250 m NDVI data: An assessment for the US Central Great Plains,” *Remote Sens. Environ.*, vol. 112, no. 3, pp. 1096–1116, 2008. doi: 10.1016/j.rse.2007.07.019.

[295] J. Dong et al., “Tracking the dynamics of paddy rice planting area in 1986–2010 through time series Landsat images and phenology-based algorithms,” *Remote Sens. Environ.*, vol. 160, pp. 99–113, Apr. 2015. doi: 10.1016/j.rse.2015.01.004.

[296] R. A. Geerken, “An algorithm to classify and monitor seasonal variations in vegetation phenologies and their inter-annual change,” *ISPRS J. Photogram. Remote Sens.*, vol. 64, no. 4, pp. 422–431, 2009. doi: 10.1016/j.isprsjprs.2009.03.001.

[297] Y. Shao, R. S. Lunetta, B. Wheeler, J. S. Iiames, and J. B. Campbell, “An evaluation of time-series smoothing algorithms for land-cover classifications using MODIS-NDVI multi-temporal data,” *Remote Sens. Environ.*, vol. 174, pp. 258–265, Mar. 2016. doi: 10.1016/j.rse.2015.12.023.

[298] R. Azar, P. Villa, D. Stroppiana, A. Crema, M. Boschetti, and P. A. Brivio, “Assessing in-season crop classification performance using satellite data: A test case in Northern Italy,” *Eur. J. Remote Sens.*, vol. 49, no. 1, pp. 361–380, 2016. doi: 10.5721/EuJRS20164920.

[299] P. Villa, D. Stroppiana, G. Fontanelli, R. Azar, and P. A. Brivio, “In-season mapping of crop type with optical and X-band SAR data: A classification tree approach using synoptic seasonal features,” *Remote Sens.*, vol. 7, no. 10, pp. 12,859–12,886, 2015. doi: 10.3390/rs71012859.

[300] C. Gómez, J. C. White, and M. A. Wulder, “Optical remotely sensed time series data for land cover classification: A review,” *ISPRS J. Photogram. Remote Sens.*, vol. 116, pp. 55–72, June 2016. doi: 10.1016/j.isprsjprs.2016.03.008.

[301] F. Waldner et al., “Towards a set of agrosystem-specific cropland mapping methods to address the global cropland diversity,” *Int. J. Remote Sens.*, vol. 37, no. 14, pp. 3196–3231, 2016. doi: 10.1080/01431161.2016.1194545.

[302] S. Skakun et al., “Early season large-area winter crop mapping using MODIS NDVI data, growing degree days information and a Gaussian mixture model,” *Remote Sens. Environ.*, vol. 195, pp. 244–258, 2017. doi: 10.1016/j.rse.2017.04.026.

[303] A. Bouvet and T. Le Toan, “Use of ENVISAT/ASAR wide-swath data for timely rice fields mapping in the Mekong River Delta,” *Remote Sens. Environ.*, vol. 115, no. 4, pp. 1090–1101, 2011. doi: 10.1016/j.rse.2010.12.014.

[304] I. Choudhury and M. Chakraborty, “SAR signature investigation of rice crop using RADARSAT data,” *Int. J. Remote Sens.*, vol. 27, no. 3, pp. 519–534, 2006. doi: 10.1080/01431160500239172.

[305] Y. Oguro, Y. Suga, S. Takeuchi, M. Ogawa, T. Konishi, and K. Tsuchiya, “Comparison of SAR and optical sensor data for monitoring of rice plant around Hiroshima,” *Adv. Space Res.*, vol. 28, no. 1, pp. 195–200, 2001. doi: 10.1016/S0273-1177(01)00345-3.

[306] Y. Shao et al., “Rice monitoring and production estimation using multitemporal RADARSAT,” *Remote Sens. Environ.*, vol. 76, no. 3, pp. 310–325, 2001. doi: 10.1016/S0034-4257(00)00212-1.

[307] P. Hao, H. Tang, Z. Chen, and Z. Liu, "Early-season crop mapping using improved artificial immune network (IAIN) and Sentinel data," *PeerJ*, vol. 6, no. 2, p. e5431, 2018. doi: 10.7717/peerj.5431.

[308] H. Jiang et al., "Early season mapping of sugarcane by applying machine learning algorithms to Sentinel-1A/2 time series data: A case study in Zhanjiang City, China," *Remote Sens.*, vol. 11, no. 7, p. 861, 2019. doi: 10.3390/rs11070861.

[309] D. Stroppiana et al., "In-season early mapping of rice area and flooding dynamics from optical and SAR satellite data," *Eur. J. Remote Sens.*, vol. 52, no. 1, pp. 206–220, 2019. doi: 10.1080/22797254.2019.1581583.

[310] M. Reynolds and F. Pinto, *Theory and Application of Phenotyping in Wheat for Different Target Environments (Advances in Crop Breeding Techniques).* Cambridge, U.K.: Burleigh Dodds Science Publishing, 2019.

[311] H. Zheng et al., "Early season detection of rice plants using RGB, NIR-GB and multispectral images from unmanned aerial vehicle (UAV)," *Comput. Electron. Agr.*, vol. 169, p. 105,223, Feb. 2020. doi: 10.1016/j.compag.2020.105223.

[312] A. Krizhevsky, I. Sutskever, and G. E. Hinton, "Imagenet classification with deep convolutional neural networks," in *Proc. Advances neural Information Processing Systems*, 2012, pp. 1097–1105.

[313] W. Zaremba, I. Sutskever, and O. Vinyals, Recurrent neural network regularization. [Online]. Available: arXiv:1409.2329, 2014.

[314] E. DeTurk, "Plant nutrient deficiency symptoms. Physiological basis," *Ind. Eng. Chem.*, vol. 33, no. 5, pp. 648–653, 1941. doi: 10.1021/ie50377a022.

[315] R. Jackson, R. Reginato, and S. Idso, "Wheat canopy temperature: A practical tool for evaluating water requirements," *Water Resour. Res.*, vol. 13, no. 3, pp. 651–656, 1977. doi: 10.1029/WR013i003p00651.

[316] J. J. Olivares-Villegas, M. P. Reynolds, and G. K. McDonald, "Drought-adaptive attributes in the Seri/Babax hexaploid wheat population," *Funct. Plant Biol.*, vol. 34, no. 3, pp. 189–203, 2007. doi: 10.1071/FP06148.

[317] R. S. Pinto, M. P. Reynolds, K. L. Mathews, C. L. McIntyre, J.-J. Olivares-Villegas, and S. C. Chapman, "Heat and drought adaptive QTL in a wheat population designed to minimize confounding agronomic effects," *Theor. Appl. Genet.*, vol. 121, no. 6, pp. 1001–1021, 2010. doi: 10.1007/s00122-010-1351-4.

[318] S. Gálvez et al., "Hotspots in the genomic architecture of field drought responses in wheat as breeding targets," *Funct. Integr. Genom.*, vol. 19, no. 2, pp. 295–309, 2019. doi: 10.1007/s10142-018-0639-3.

[319] M. Gutierrez, M. P. Reynolds, W. R. Raun, M. L. Stone, and A. R. Klatt, "Spectral water indices for assessing yield in elite bread wheat genotypes under well-irrigated, water-stressed, and high-temperature conditions," *Crop Sci.*, vol. 50, no. 1, pp. 197–214, 2010. doi: 10.2135/cropsci2009.07.0381.

[320] X. Li et al., "Spectral difference analysis and airborne imaging classification for citrus greening infected trees," *Comput. Electron. Agr.*, vol. 83, pp. 32–46, Apr. 2012. doi: 10.1016/j.compag.2012.01.010.

[321] M. Jansen, S. Bergsträsser, S. Schmittgen, M. Müller-Linow, and U. Rascher, "Non-invasive spectral phenotyping methods can improve and accelerate cercospora disease scoring in sugar beet breeding," *Agriculture*, vol. 4, no. 2, pp. 147–158, 2014. doi: 10.3390/agriculture4020147.

[322] B. Qiu, W. Li, Z. Tang, C. Chen, and W. Qi, "Mapping paddy rice areas based on vegetation phenology and surface moisture conditions," *Ecol. Indicat.*, vol. 56, pp. 79–86, Sept. 2015. doi: 10.1016/j.ecolind.2015.03.039.

[323] M. Guérif and C. Duke, "Calibration of the SUCROS emergence and early growth module for sugar beet using optical remote sensing data assimilation," *Eur. J. Agron.*, vol. 9, no. 2–3, pp. 127–136, 1998. doi: 10.1016/S1161-0301(98)00031-8.

[324] C. Atzberger, "Advances in remote sensing of agriculture: Context description, existing operational monitoring systems and major information needs," *Remote Sens.*, vol. 5, no. 2, pp. 949–981, 2013. Doi: 10.3390/rs5020949.

[325] M. J. Pinthus, "Lodging in wheat, barley, and oats: The phenomenon, its causes, and preventive measures," *Adv. Agron.*, vol. 25, pp. 209–263, 1974. doi: 10.1016/S0065-2113(08)60782-8.

[326] R. Fischer and M. Stapper, "Lodging effects on high-yielding crops of irrigated semidwarf wheat," *Field Crops Res.*, vol. 17, no. 3–4, pp. 245–258, 1987. doi: 10.1016/0378-4290(87)90038-4.

[327] F. Hosoi and K. Omasa, "Estimation of vertical plant area density profiles in a rice canopy at different growth stages by high-resolution portable scanning lidar with a lightweight mirror," *ISPRS J. Photogram. Remote Sens.*, vol. 74, pp. 11–19, Nov. 2012. doi: 10.1016/j.isprsjprs.2012.08.001.

[328] F. Baret, V. Houles, and M. Guérif, "Quantification of plant stress using remote sensing observations and crop models: The case of nitrogen management," *J. Exp. Bot.*, vol. 58, no. 4, pp. 869–880, 2007. doi: 10.1093/jxb/erl231.

[329] T. Murakami, M. Yui, and K. Amaha, "Canopy height measurement by photogrammetric analysis of aerial images: Application to buckwheat (Fagopyrum esculentum Moench) lodging evaluation," *Comput. Electron. Agr.*, vol. 89, pp. 70–75, Nov. 2012. doi: 10.1016/j.compag.2012.08.003.

[330] B. W. Fitch, R. L. Walraven, and D. E. Bradley, "Polarization of light reflected from grain crops during the heading growth stage," *Remote Sens. Environ.*, vol. 15, no. 3, pp. 263–268, 1984. doi: 10.1016/0034-4257(84)90036-1.

[331] Z. Liu et al., "Comparison of spectral indices and principal component analysis for differentiating lodged rice crop from normal ones," in *Proc. Int. Conf. Computer and Computing Technologies Agriculture*, 2011, pp. 84–92.

[332] F. Kogan, W. Guo, and W. Yang, "Drought and food security prediction from NOAA new generation of operational satellites," *Geomatic., Natural Hazards Risk*, vol. 10, no. 1, pp. 651–666, 2019. doi: 10.1080/19475705.2018.1541257.

[333] N. Yu, L. Li, N. Schmitz, L. F. Tian, J. A. Greenberg, and B. W. Diers, "Development of methods to improve soybean yield estimation and predict plant maturity with an unmanned aerial vehicle based platform," *Remote Sens. Environ.*, vol. 187, pp. 91–101, Dec. 2016. doi: 10.1016/j.rse.2016.10.005.

GRS